RADC-TDR-62-491
ASTIA Document No. AD-

TRG-168-TDR-1
30 November, 1962

TECHNICAL NOTE

on

HETERODYNE DETECTION IN OPTICAL COMMUNICATION

Edited by:

James LaTourrette

Project Leader:

Stephen Jacobs

TECHNICAL RESEARCH GROUP, INC.
2 Aerial Way
Syosset, New York

TRG Contract No. 168

Contract No. AF30(602)-2591
Project No. 4519
Task No. 451905

Prepared for

ROME AIR DEVELOPMENT CENTER
AIR FORCE SYSTEMS COMMAND
UNITED STATES AIR FORCE
GRIFFISS AIR FORCE BASE
NEW YORK

NOTICES

When Government drawings, specifications, or other data are used for any purpose other than in connection with a definitely related Government procurement operation, the United States Government thereby incurs no responsibility nor any obligation whatsoever; and the fact that the Government may have formulated, furnished, or in any way supplied the said drawings, specifications or other data, is not to be regarded by implication or otherwise as in any manner licensing the permission to manufacture, use or sell any patented investion that may in any way be related thereto

---

Qualified requesters may obtain copies of this report from the ASTIA Document Center, Arlington Hall Station, Arlington 12, Virginia. ASTIA services for the Department of Defense contractors are available through the "Field of Interest Register" on a "Need-to-know" certified by the cognisant military agency of their project or contract.

Copies of RADC Technical Reports and Technical Notes should not be returned to Rome Air Development Center unless return is required by security considerations, contractual obligations, or notice on a specific document.

ASTIA release to OTS is not authorized.

TECHNICAL RESEARCH GROUP

RADC-TDR-62-491
ASTIA Document No. AD-

TRG-168-TDR-1
30 November 1962

TECHNICAL NOTE

on

HETERODYNE DETECTION IN OPTICAL COMMUNICATION

Edited by:
James LaTourrette

Project Leader:
Stephen Jacobs

TECHNICAL RESEARCH GROUP, INC.
2 Aerial Way
Syosset, New York

TRG Contract No. 168

Contract No. AF30(602)-2591

Prepared for

ROME AIR DEVELOPMENT CENTER
AIR FORCE SYSTEMS COMMAND
UNITED STATES AIR FORCE
GRIFFISS AIR FORCE BASE
NEW YORK

FOREWORD

This report was prepared by TRG, Inc., Syosset, New York, on Air Force Contract AF30(602)-2591 under Task No. 451905 of Project No. 4519, "Theoretical and Experimental Investigation of Broadband Coherent Optical Communication Techniques". The work was administrated under the direction of the Directorate of Communications, Advanced Development Laboratory, Advanced Communications Techniques Branch, Rome Air Development Center. Mr. Jesse Kaufman was Project Engineer for the Directorate.

This investigation is an effort of the Radio and Optical Spectroscopy Laboratory of TRG, Inc. Dr. Gordon Gould, assisted by Dr. James LaTourrette, is responsible for research activity at the Technical Research Group. The Project Leader of this investigation is Dr. Stephen Jacobs.

This Technical Report was edited by Dr. LaTourrette; the principal authors were Dr. LaTourrette, Dr. Jacobs, Dr. Gould, and Mr. Paul Rabinowitz. The Report covers the first nine months of work on Contract No. AF30(602)-2591. Work on this contract is closely correlated with work being carried out under Contract No. AF33(657)-8060, devoted to the stabilization of LASERs for optical heterodyne detection.

The authors wish to express their appreciation to Dr. Richard Daly for many helpful discussions, to Dr. Maurice Newstein and Dr. Nicholas Solimene for contributions to the theory of optical heterodyning, and to Mr. John Poulos and Mr. Bert Freeman for technical assistance.

TECHNICAL RESEARCH GROUP

ABSTRACT

The properties of optical heterodyne detection are analyzed and measured using a LASER and a Twyman-Green interferometer. It is shown that heterodyne amplification preserves the signal-to-noise ratio in the detected difference frequency in the presence of incoherent noise. The uses of heterodyne detection in optical communication, demultiplixing of channels, demodulation of FM and AM, Doppler and displacement measurements, and stabilization of LASERs is discussed. The elements of an optical communication link are discussed: LASERs, modulators, transmission path, and detectors. Recommendations are made for future work.

HETERODYNE DETECTION IN OPTICAL COMMUNICATION

TABLE OF CONTENTS

TABLE OF CONTENTS (Continued)

ILLUSTRATIONS

TABLES

1.0 Introduction

This Technical Report describes the "State-of-the-Art" of optical communication--particularly of heterodyne demodulation. Progress is reported in the first 9 months of a "Theoretical and Experimental Investigation of Broadband Coherent Optical Communication Techniques", (RADC Contract No. AF30(602)-2591). The emphasis in this study has been "placed upon temporally and spatially coherent detection techniques for receiver equipment" -- that is, upon optical heterodyne detection.

1.1 Epitome

In optical heterodyne detection, a LASER local oscillator beam is made spatially and temporally coherent with an incoming signal beam. A current at the difference frequency of the coincident beams is generated in the nonlinear process of photo-detection. This heterodyne signal current and the RMS shot noise current are both proportional to the square root of local oscillator power. Thus the signal-to-noise ratio inherent in the signal beam is preserved, while the incoherent background noise is submerged.

The primary purposes of the investigation are:

a. To determine how well the predicted and observed properties of optical heterodyne detection agree.

b. To show how optical heterodyne detection can be used to advantage in optical communication and other applications.

During the first 9 months of the contract the following steps were taken toward the objectives:

a. The theory of heterodyning was refined and applied to single-sideband, AM, and FM detection; the expected signal-to-noise ratios were calculated.

b. The fluctuations in the photo-emitted current generated by a LASER were measured between 10 cps and 10^8 cps. As predicted, the fluctuations did not exceed shot noise. This is essential if the signal-to-noise ratio is to be preserved in heterodyne detection.

c. Amplitude- and phase-modulated light beams were homodyne-detected.

d. Heterodyne amplification of a light signal was observed as predicted.

e. Signal-to-noise measurements under a variety of conditions were initiated but not yet completed.

In this investigation an experimental technique is being used which simplifies the maintenance of coherence (see Section 2.4.3.3). The beam from a single LASER is split by a Twyman-Green interferometer into "local oscillator beam" and a "signal beam". A photograph of the experimental arrangement is shown in Figure 1.1-1. After the signal beam has been modulated and otherwise altered, the two beams are rejoined at the detector for signal and noise measurements. Even though the oscillator frequency drifts, only an electrically adjustable phase difference exists between "local oscillator" and "signal carrier" beams.

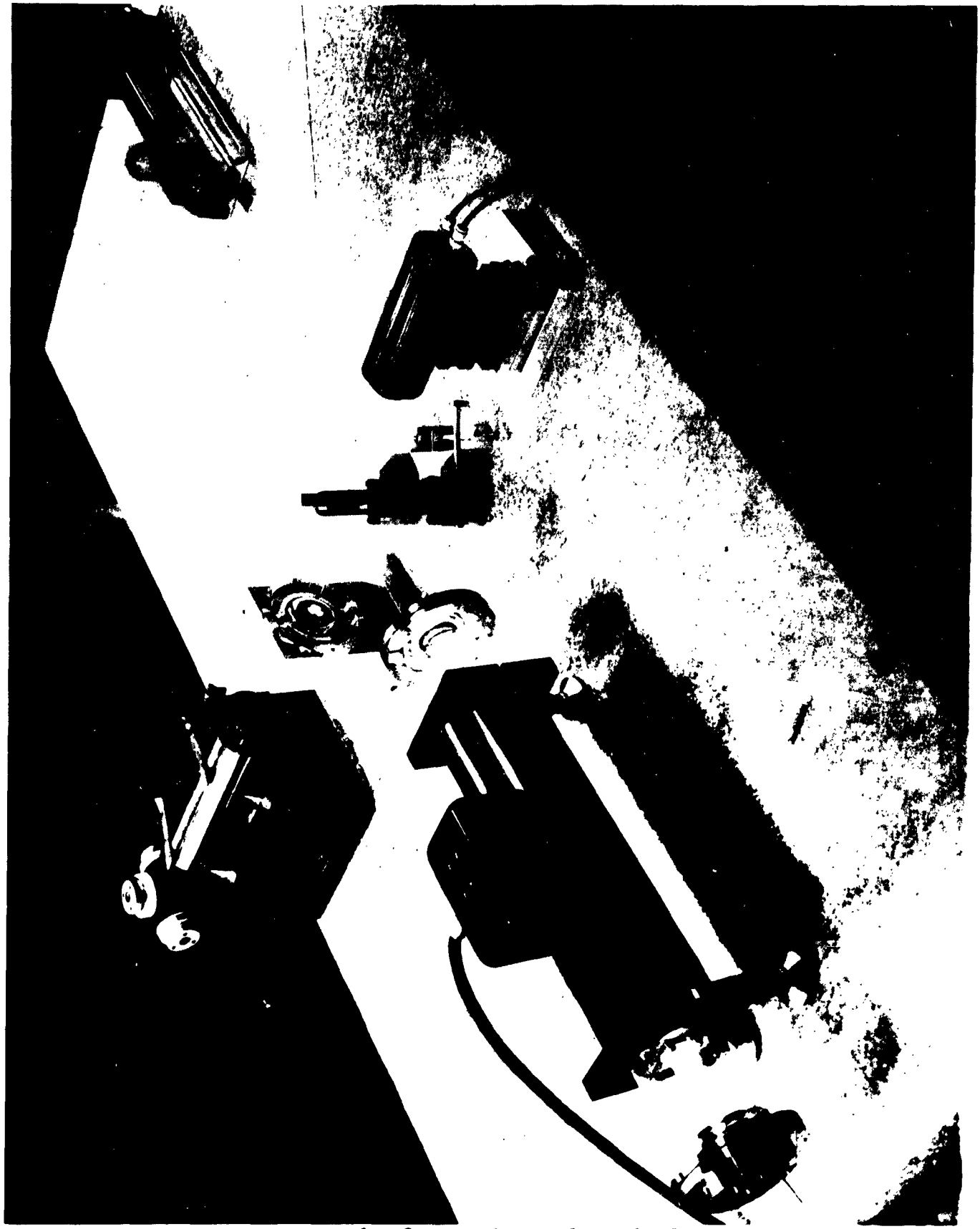

Fig. No. 1.1-1 Photograph of Experimental Optical Homodyne System

The problems of LASER self-stabilization and phase-locking one LASER with another are being solved in a parallel program, (Contract No. AF33(657)-8060). LASERs oscillating at a single frequency in a single spatial mode were developed for this purpose under Contract No. AF49(638)-673.

During the first 9 months of the investigation no difficulties have arisen which would negate the advantages of optical heterodyne detection. The predicted phenomena have been observed and spatial coherence has been readily achieved in the laboratory.

The transmitters and modulators required for optical communication are also under intensive development. At present, the principle uncertainty in predicting the capability of a system is the effect of atmospheric fluctuations and dispersion on the beam. Therefore an optical communication link should be established to gain experience with an atmospheric transmission path.

1.2 Optical Communications

The appropriate starting point for any communications study is Shannon's fundamental expression for the maximum information transfer capacity through a channel in the presence of noise:

$$C = \Delta f \ln(1 + S/N) \qquad (1.2\text{-}1)$$

where

C = information capacity in (bits/sec) when the logarithm is taken to the base 2,

Δf = channel bandwidth in (cycles/sec),

S/N = signal-to-noise power ratio.

To achieve the optimum information capacity, described in Eq. 1.2-1, very sophisticated coding techniques would be required. For error-free transmission by conventional coding techniques, $S/N > 30$, and in practice, $C \approx \Delta f$.

The irreducible "noise-in-signal" is the shot noise in the photocurrent of a perfect quantum detector. It then follows (see Section 2.4.1.1) that the maximum possible signal-to-noise power ratio is

$$i_s^2/\overline{i_n^2} = S/N = \frac{\text{(no. of photoelectrons per sec.)}}{2\Delta f} \qquad (1.2\text{-}2)$$

$$= \frac{\eta \text{ (no. of photons per sec.)}}{2\Delta f} \qquad (1.2\text{-}3)$$

where η = quantum efficiency of the detector
= (no. of photoelectrons per photon)

Thus the information capacity and the usable bandwidth are directly proportional to the beam power. For a given information capacity, the transmitted power required will increase in proportion to any noise added to the shot noise in all components of the communications link and with the attenuation.

It is shown in Section 2.4 that minimum power is required in a perfectly coherent system; i.e., the light is generated, transmitted, and detected in a single mode. The advent of the LASER makes possible an approach to this ideal at optical frequencies.

The components of a link are discussed in succeeding sections. They are:

Oscillators: CW gaseous LASERs have been made to oscillate in a single mode while radiating 10^{16} photons/sec (1 milliwatt). This would provide an information capacity of $\sim 10^{15}$ bits/sec if all other components were "perfect" (Equations 1.2-1, -2, -3). Radiation in a single spatial mode, or "Fraunhofer cone", implies the maximum power per unit solid angle permitted by diffraction (perfect spatial coherence).

Theory indicates that the power fluctuations in the beam of a LASER, oscillating at a single, fixed frequency, should not exceed "photon shot noise" (perfect temporal coherence). Our measurements show that this is true of existing LASERs. A program is in progress at TRG to stabilize LASERs in single-mode oscillation under field as well as laboratory conditions.

Modulators: A Pockels-cell electro-optical modulator with a CW bandwidth, $\Delta\nu = 10^9$ cycles/sec, recently has been announced. Although theoretically feasible, it may not be worth while to go beyond this, since channel bandwidths are limited by atmospheric or other dispersion and by microwave terminal equipment. Multiplexing high bit-rate channels is more easily accomplished by optical than by microwave techniques, since the fractional bandwidths are smaller. The maximum channel bandwidth allowed by dispersion may be achieved by single sideband modulation or by using detectors which correct for the phase shift between two sidebands; it is not yet clear which technique is superior.

The spatial coherence of the beam must be preserved through the modulator. While exacting, this requirement is not more difficult than generating a single mode or diffraction limited beam.

Amplitude, phase, polarization, or single-sideband modulation are all possible. The relative merits of each are yet to be fully evaluated.

Transmission Path: Cable links are quite different from free space links; repeaters can be freely used in the former while power must be conserved in the latter. In the latter case, then, single mode operation is important. The present study is restricted to such highly coherent systems.

The dispersion and fluctuation properties of the atmosphere are essential design parameters. Results of several investigations at other laboratories are not yet available. Our own observation

is: phase fluctuations as large as $\pi/2$ occur in path lengths of the order of 1 meter.

Demodulators: Noise and attenuation are serious problems in detection. A quantum conversion efficiency, $\eta < 1$, is an attenuation which must be made up in initial power. Semiconductor detectors exhibit η's ~ 1, while photoemitters have η's $\simeq 0.1$. On the other hand, the background noise due to dark current in semiconductor photo-conductors is much larger than in photoemissive detectors. We have shown theoretically that, if the local oscillator has sufficient power, heterodyne detection can raise the signal above any other noise incoherent with the signal. One of the principle objectives of the contract is to quantitatively validate this statement experimentally.

1.3 Optical Heterodyne Detection

In heterodyne detection, interfering signal and local oscillator waves are applied to a non-linear detector element. Among the Fourier components of the detector output are frequencies not present in the original waves. In particular, the beat frequency is present and serves as the signal.

In a "square-law" detector, the original signal-to-noise-in-signal ratio is preserved in the beat frequency signal, no matter how large the (single-mode) heterodyne power. By a square-law detector is meant one which responds in proportion to the square of the interfering fields or currents as the case may be. All photo detectors are square-law in this sense.

Heterodyne detection at the photo-detector of interfering signal and spatially coherent narrow-band local oscillator fields increases both the effective signal and noise in proportion. The effect corresponds precisely to heterodyne detection of a radio frequency signal. This important result is derived briefly below.

Let the field at the photo-sensitive surface be

$$\mathcal{E} = E_{lo}\cos(\omega_{lo}t) + E_s\cos(\omega_s t) \qquad (1.3\text{-}1)$$

where

E_{lo} = local oscillator field amplitude

E_s = signal field amplitude

$\omega_{lo} = \omega_s$ = respective angular frequencies.

If we average over a response time, τ, such that

$$\Delta\omega = (\omega_{lo} - \omega_s) < \frac{1}{\tau} << \omega_{lo} \approx \omega_s \qquad (1.3\text{-}2)$$

optically equal

Then

$$\overline{\mathcal{E}^2} = \frac{1}{2} E_{lo}^2 + E_{lo}E_s \cos(\omega_{lo} - \omega_s)t + \frac{1}{2} E_s^2 \qquad (1.3\text{-}3)$$

The resulting alternating component of the photocurrent at the difference frequency is

$$i_{\text{peak AC}} = \frac{2E_sE_{lo}}{E_{lo}^2 + E_s^2} i_{DC} \qquad (1.3\text{-}4)$$

and if $E_s << E_{lo}$,

$$\overline{i_{AC}^2} = 2\left[\frac{E_s}{E_{lo}}\right]^2 i_{DC}^2 = 2\frac{P_s}{P_{lo}} i_{DC}^2 \qquad (1.3\text{-}5)$$

and

$$i_{DC} = \frac{\eta e P_{lo}}{h\nu} \qquad (1.3\text{-}6)$$

where P_{lo} = local oscillator power. On the other hand the shot noise is given by

$$\overline{i_N^2} = 2ei_{DC}\Delta f \qquad (1.3\text{-}7)$$

Therefore, if the local oscillator generates only shot noise in the detector,

$$\frac{\overline{i_{AC}^2}}{\overline{i_N^2}} = \frac{\eta P_s}{h\nu\Delta f} \tag{1.3-8}$$

or

$$\boxed{S/N = \frac{\eta(\text{no. of signal photons per sec})}{\Delta f}} \tag{1.3-9}$$

which is independent of the impinging local oscillator power, P_{lo}. For $\omega_{lo} \neq \omega_s$, the detector bandpass, Δf, must be twice as large as the Δf required for direct detection (Eq. 1.2-3) with the same information bandwidth. Thus, Eq. 1.3-9 gives just the maximum signal-to-noise ratio which can be obtained in the absence of background noise. For homodyne detection, ($\omega_{lo} = \omega_s$), a factor of two improvement in S/N can, in principle, be achieved.

The advantage of signal detection together with a spatially and temporally coherent local oscillator field is that the local oscillator field may in principle be made arbitrarily large without affecting S/N. Thus, signal and noise-in-signal output currents are increased proportionately while the incoherent background noise currents are unaffected. To achieve optimum channel capacity, it is only necessary that the shot noise of the photo-current, due to the local oscillator, exceed the background noise. This is possible with available CW LASER power even for IR photo conductive detectors.

In the above analysis, the signal consisted of just one frequency offset from the local oscillator. This is equivalent to a single sideband with suppressed carrier. If two sidebands are present (AM or FM) a local oscillator can also be used to demodulate with the same advantage (see Section 2.4.3.1).

In summary, heterodyne mixing of coherent local oscillator and signal beams on a square-law detector generates an amplified signal at the beat frequency. The properties of this phenomenon can serve several useful purposes, which are discussed in later sections:

A. The signal-to-noise ratio inherent in the signal beam is preserved in detection. This is accomplished by

1. Raising the signal level above the detector noise level.

2. Amplifying only that light which is coherent with or falls within the Fraunhofer cone of the local-oscillator (spatial filtering).

3. Passing only the photocurrent generated by light whose frequency difference with the local oscillator is within the receiver band (temporal filtering).

Preservation of S/N is most useful and striking when the signal power and bandwidth are small.

B. Multiplexed channels, stacked within a total band not exceeding a microwave frequency, can be separated by bandpass filters following the detector. This becomes possible if the beats with a local oscillator are stronger than the beats between the channels. An alternative technique is the separation of widely spaced channels by optical band pass-filters.

C. FM, AM, single-sideband, and polarization-modulated signals can all be heterodyne-demodulated.

D. Doppler shifts in a reflected signal can be measured.

E. Displacement of a distant reflector can be measured to a fraction of a wavelength.

F. Stabilization of the oscillation frequency of a LASER with respect to its own fluorescent line or with respect to another oscillator or signal can be achieved.

2.0 The Elements of an Optical Communication System

2.1 LASERs for Optical Heterodyning

It will be shown, in the section on optical modulation techniques (2.2.1), that single-mode LASER operation is essential to maximum information capacity in an optical heterodyne communications system. In addition, it is shown in the discussion on optical heterodyne detection (2.4.3) that an optical heterodyne system can, in general, be in tune for a single frequency only. These considerations of information capacity and optical demodulation, combined with the heterodyne S/N equation, Eq. (1.3-9), dictate the selection of an optimum LASER for optical heterodyning.

In choosing between LASERs of comparable single-mode power, Eq. (1.3-9) indicates that the lowest frequency LASER, with the most photons per unit power, gives better S/N, (at least out to a limit of $h\nu \approx kT$, where thermal noise power from the environment is comparable to the signal beam power, e.g., for $T = 300°K$, $\lambda = \frac{hc}{kT} \approx 50\mu$).

2.1.1 Considerations Leading to Large Single-Mode Power

Two characteristics of a LASER medium which contribute to large single-mode beam power are Doppler width and gain. Referring to the figure below, a LASER can, in general, oscillate in modes corresponding to every frequency within the fluorescence line for which the cavity is resonant. When more than one cavity

mode lies within the fluorescent line profile, single-mode operation can be achieved only by operating so close to threshold that only the highest-gain mode can sustain oscillation. This means of operation clearly falls short of optimum power, since it must be achieved either by drastically reducing pumping power or by increasing losses.

Techniques for obtaining high power in a single axial mode include:

a. Reducing the fluorescence linewidth,

$$\Delta\nu_{Doppler} \sim \frac{1}{\lambda}\sqrt{\frac{T}{M}}$$ where T is the absolute temperature
M is the atomic weight
λ is the wavelength.

i.e., choose long wavelengths, heavy elements and/or low temperatures.

b. Separating cavity modes.

Separation, $\Delta\nu = \frac{c}{2L}$, depends only on cavity length. The minimum value of L is set by the balance between LASER gain and cavity losses. Therefore, it is desirable to work with high-gain LASER media to facilitate large cavity mode separations.

c. Inhibiting oscillation at undesired frequencies with a third Fabry-Perot reflector.*

Finally, two more factors influence the choice of a LASER for optical heterodyning. These involve the State-of-the-Art of radiation

---

*D.A. Kleinman and P.P. Kisliuk, BSTJ, 41, 453 (1962).

detectors and are not fundamental to the heterodyne process, but are, rather, practical considerations: In order to have a large information capacity, Δf, and to make the detection quantum efficiency, η, large, it is necessary that detectors be available which have short response times and high quantum efficiency at the LASER frequency. These detector parameters are summarized in Section 2.4.1.

Table 2.1-1 lists several continuous wave LASERs, with their operating wavelengths, approximate gain per meter, and approximate power per unit volume. The table indicates that the various gaseous systems are capable of a similar order of magnitude in output power. One representative, high-powered, solid-state LASER is listed to show the potentiality of this class of LASERs. It remains to be seen, however, whether the very serious obstacles to single-mode operation can be surmounted in the future.

2.1.2 Choice of a LASER for the Present Work

The present work has centered around the use of the 1.15μ He-Ne LASER, because it was the only continuous wave LASER available at the time this work began. The maximum single-mode power obtainable is very small because no provision for mode selection has yet been incorporated into the LASER and the only way to obtain single-mode output is to cut down the rf power. The present work has, moreover, been restricted to photoemissive detection, where the highest available detector quantum efficiency is that of the S-1 photoemissive surface, $\eta_{max}(\lambda = 1.15\mu) \leq 10^{-4}$.

Table 2.1-1

Power of Several LASERs

LASER	λ (microns)	Gain (meter^{-1})	Power density (mw/cm^3) (7mm ID cavity)
He-Ne	.6328	.015	>0.3
(internal discharge)	1.15	.12	0.43
	3.39	158.*	>0.1
He-Xe	2.026	2.71	>0.1
(internal discharge			
Cs-He	3.20	.15	>0.1
(optically pumped)	7.18	1.	0.1
CaF_2(Dy^{++}doped)	2.36	2.71	120
(optically pumped crystal)			(5 cm, 3/16" dia. rod)

---

*William R. Bennett, Jr., Private Communication.

The 1.15μ He-Ne LASER used in the present work consists of a 7mm ID Plasma Tube and a near-confocal resonator, (flat vs 396 cm sphere, separated by 123.8 cm). The total beam power is 1250μw, and must be reduced to 6μw in order to excite only one mode (no transverse modes; single axial mode). The beam emerges from the LASER through the flat reflector at which point the beam diameter measures approximately 1.5mm.

The cavity modes of the LASER were investigated by observing beat frequencies with a spectrum analyzer. In addition to c/2L modes, observed at 120,240,360, and 480 Mc, a great many angular modes were detected when the LASER was operating at full power. These were spaced approximately 23 Mc apart, on either side of the c/2L frequencies (see Fig. 2.1-1).

According to the analysis of Boyd and Gordon*, the spacing of the angular modes is

$$\Delta\nu_{angular} = \left(\frac{c}{2L}\right)\frac{1}{2L}\cos^{-1}\left(1 - \frac{2L}{b_1}\right) = 22.6 \text{ Mc}$$

where b_1 is the radius of the spherical reflector, and L is the separation of the two reflectors.

2.1.3 Improved LASERs for Use in Optical Heterodyning

A. Photoemissive Detection. The highest quantum efficiency in photoemissive detectors occurs in the wavelength region $\lambda < 6000\text{Å}$, ($\eta > .1$). This consideration points to the use

---

*G.D. Boyd and H. Kogelnik, BSTJ 41, July 1962 (p. 1361).

FIG. 2.1-1

MULTIMODE He-Ne LASER WITH NEAR-CONFOCAL RESONATOR

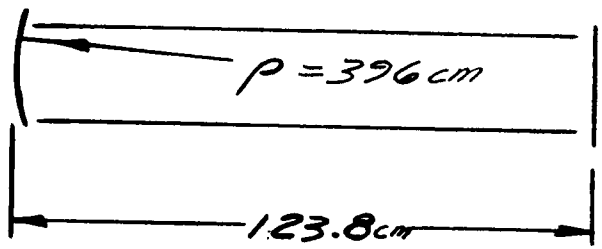

a)

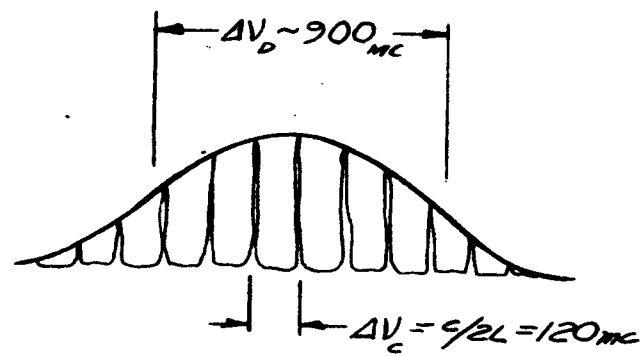

b) OBSERVED FREQUENCY SPECTRUM

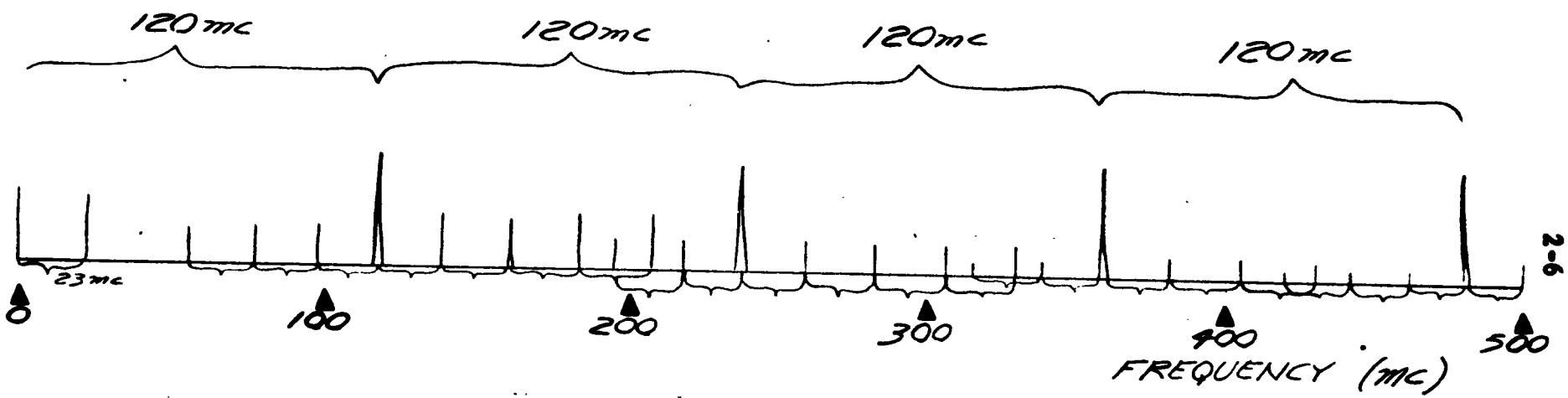

of the 6328Å He-Ne LASER which is, at the time of writing, the shortest wavelength LASER of moderate power output. Single-mode powers of the order of 10 milliwatts are obtainable, based on recent reports of total power (20 mw total beam power reported by the Perkin-Elmer Corp.) provided a suitable optical cavity is used, (3-mirror interference system*).

It will be recalled (Eq. 1.3-9) that the ultimate signal-to-noise achievable in broadband heterodyne system is

$$S/N \propto \eta(\text{single-mode photon rate}).$$

Thus, compared to the present work at $\lambda = 1.15\mu$ with $6\mu w$ of single-mode power, the above system would facilitate an improvement in S/N of about 10^3 in detective quantum efficiency and 10^3 in incident single-mode photon rate, a factor of 10^6 in all. A further great advantage of a visible LASER is the convenience of being able to see the LASER output while aligning optical elements.

B. Photovoltaic and Photoconductive Detection.

The high-gain xenon LASER ($\lambda = 2.026\mu$) has a single-mode output power of the order of 1mw** without requiring any optical mode selector. More than ten times this power is probably obtainable.

---

* D.A. Kleinman and P.P. Kisliuk, BSTJ, 41, 453 (1962).

** C.K.N. Patel, W.R. Bennett, Jr., W.L. Faust, and R.G. McFarlane, Phys. Rev. Let. 9, 102 (1962)

Moreover, the number of photons per unit power is 3 times that of the 6328Å LASER. Finally, the available detector quantum efficiency of the detector is $\eta \approx 1$.

Thus, compared to the 1.15μ 6μw He-Ne LASER with photoemissive detection, use of the xenon LASER and a photovoltaic detector facilitates an improvement in S/N of about 10^4 in quantum efficiency and 3000 in incident photon rate, a total factor of 3×10^7 overall S/N improvement.

2.2 Modulation of LASER Beams

2.2.1 Suitability of Optical Modulators

The following is a list of criteria which are important in choosing a modulator for LASER light beams in a broadband optical heterodyne system:

1. Bandwidth capability.

   $\Delta f \sim 10^9$ cps. Transmission band must be kept free of carriers in the region $f_o \pm \Delta f$, in order to avoid interference with transmitted information.

2. Distortion of signal.

   Optical surfaces and homogeneity of the modulator medium must not seriously reduce the information content of the beam. Signal must not be distorted by nonlinearities in the modulation mechanism.

3. Modulation power required.

   This must be kept reasonably small to avoid thermal distortions as well as for practical limitations.

4. Nature of the modulation process.

5. Types of LASERs whose output is to be modulated.

6. Modulation efficiency.

   Modulation must be appropriate to the LASER wavelength and pumping mechanism, e.g., transparency of optical materials, etc.

7. Other system requirements for a given modulation type.

2.2.2 Modulation Techniques

2.2.2.1 Modulation of LASER

The output of a LASER can be modulated by modulating the LASER driving power or by modulating the cavity resonance. These techniques are limited in bandwidth and are thus not in general applicable to a broadband optical communication system. It is of interest, however, to note that, for some practical applications, available power may limit the usable bandwidth so that cavity modulation techniques may be used. The simplest means for modulating the cavity is to physically move the resonator mirrors. Since no extra modulating element is required, the problems of optical perfection of the modulating medium are largely circumvented.

To give some idea of the bandwidth limitation imposed by a practical gaseous LASER, the 1.15μ He-Ne LASER requires for oscillation a cavity bandwidth $\Delta\nu \leq 1$ mc (see Section 2.2.4.1). The need for high-Q cavities, to support LASER oscillation, is at cross purposes with the desire for broadband modulation. One cannot modulate with a bandwidth greater than the cavity bandwidth. The existence of high-gain LASERs, which can sustain oscillation in a low-Q cavity, will allow the largest possible information bandwidth, (e.g., LASERs presently exist whose gain is nearly 100 times that of the 1.15μ He-Ne LASER).

2.2.2.2 Methods for Modulating Beam After it is Emitted from LASER Oscillator

Post modulation of the LASER beam does not involve the bandwidth limitation of the high-Q LASER cavity. In

addition, these methods must be used for a single-LASER transreceiver homodyne system which is being experimentally investigated.

A. Phase Modulation. Control of the retardation or advancement of a phase front is generally achieved either by altering the refractive index of a medium or by physical motion of an optical element. Phase (or frequency) modulation can be detected only with optical heterodyne techniques (see Section 2.4.3) or by means of an optical discriminator.* Therefore, this type of modulation would be difficult to observe by unauthorized observers.

B. Amplitude Modulation. In addition to the many methods for modulating the transmittance of an optical system (mechanical chopping or deflection, variable reflectivities, etc.), amplitude modulation can also be produced by modulation of phase, in conjunction with the use of polarizers.

Amplitude modulation can be detected in a straightforward way with conventional square-law detectors.

C. Polarization Modulation. All techniques for polarization modulation are merely variations of phase modulation. For example, in the amplitude modulation scheme mentioned above, if the polarizer is omitted from the transmitter output and inserted

---

*Harris, S.E. and Siegman, A.E., "A Proposed FM Phototube for Demodulating Microwave-Frequency-Modulated Light Signals", IRE Trans. on Electron Devices, Vol. ED-9, 322 (1962).

See also, Harris, S.E., "The Birefringent Discriminator", NEREM 1962.

in the detector the result is polarization modulation.* Because the coherence condition for interference of two light beams includes coherence in polarization, this form of modulation can be directly detected by optical heterodyning (with a polarized LASER local oscillator) without the need for inserting a polarizer in the path of the signal beam.

2.2.2.3 Production of Single Sideband Suppressed Carrier Optical Modulation

Single sideband suppressed carrier modulation of a LASER beam provides a solution to the problem of shifting the essentially fixed frequency of a LASER beam to another frequency, without introducing additional frequency components. It is also of interest for improving signal-to-noise ratio, for conserving bandwidth, and for propagating a signal through a dispersive medium, (see Section 2.4.3.3).

A method for producing single sideband suppressed carrier modulation at optical frequencies was originally proposed** in 1883. The principle of the method is that a rotating birefringent plate acts upon a circularly polarized light beam to produce a separable component shifted in frequency. The analysis given below shows that 100% efficiency (i.e., unit modulation transfer characteristic) can be obtained with a rotating half-wave plate. However, the physical rotation of an optical element severely limits the available information bandwidth.

---

*Blattner, D.J. and Storzer, F., "Heterodyne Receivers for R-F Modulated Light Beams", RCA Review, p. 408, Sept. 1962.

**Righi, M.A., J. Physique et Radium, 2, 437, (1883).

This limitation can be raised by using a pair of appropriately phased birefringent plates to simulate the action of a rotating plate.* For example, the Pockels electro-optic effect in KH_2PO_4 can produce an oscillating birefringence at a frequency exceeding 9 Gc/sec.** We must note, however, that a pair of oscillating birefringent crystals cannot exactly duplicate the action of a single rotating plate. As a result, at most 67% of the power can be transferred from the carrier to the single sideband in the latter case. However, little power is transferred into higher harmonics, and the carrier can still be suppressed by means of a circular polarization analyser.

The arrangement for obtaining the ideal situation of 100% conversion of carrier to single sideband is shown in Fig. 2.2-1a. A $\lambda/4$ wave plate is oriented so as to convert an incoming plane polarized LASER beam into, for example, right hand circularly polarized light. The beam then passes through a rotating $\lambda/2$ plate or, more generally, a birefringent plate which produces a phase retardation of

$$2\beta = \frac{2\pi \ell}{\lambda} (n_x - n_y) \quad ,$$

---

* Buhrer, et al, Proc. IRE, 50, 1827, (1962).

** Kaminow, I.P., Phys. Rev. Letters 6, 528 (1961).

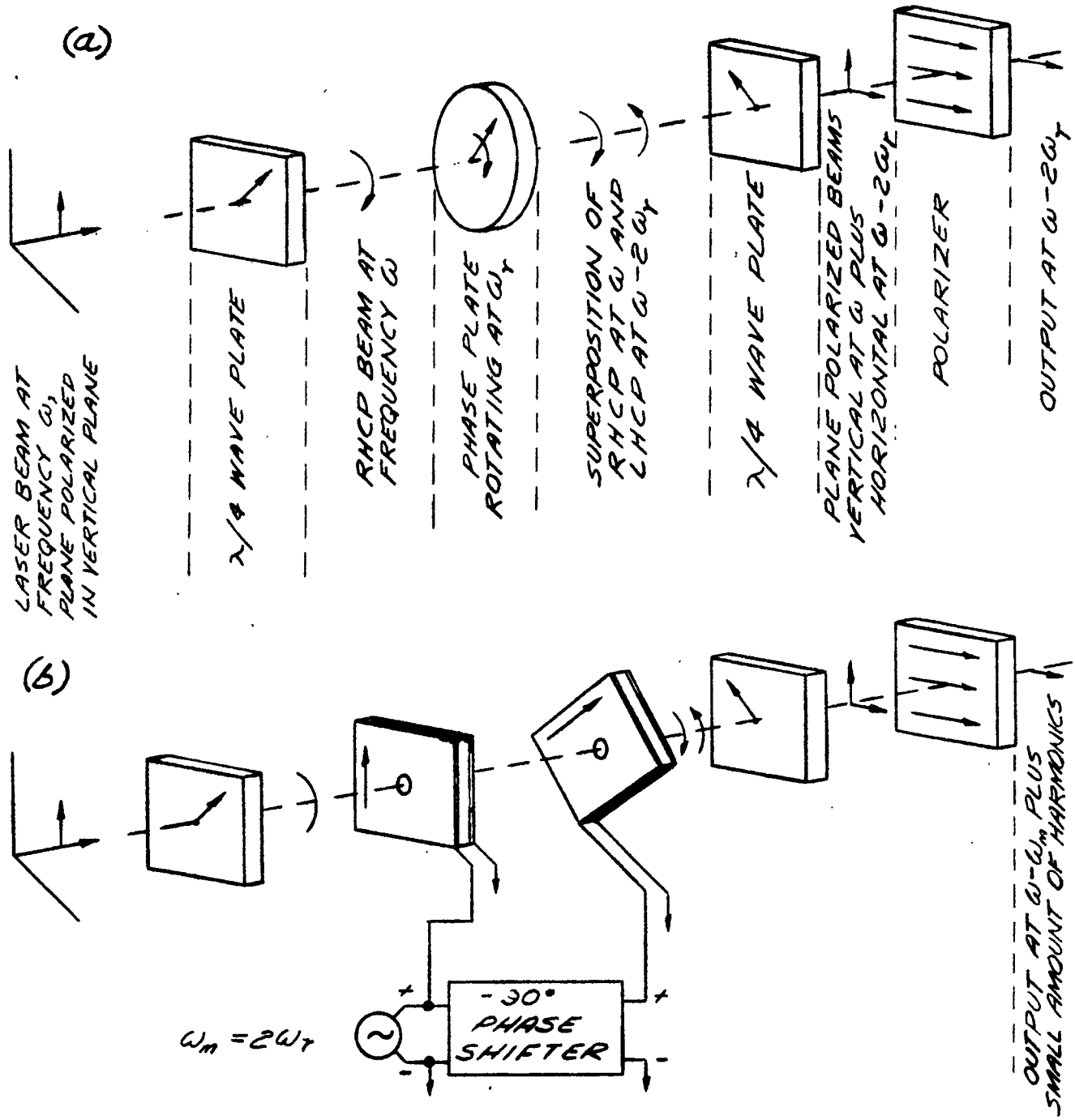

FIGURE 2.2-1. SINGLE SIDEBAND SUPPRESSED CARRIER OPTICAL MODULATOR (a) WITH ROTATING PHASE PLATE (b) WITH TWO PHASED KH_2PO_4 CRYSTALS.

and finally through a second $\lambda/4$ wave plate which converts the circularly polarized output back to plane polarization. If $\beta \neq \pi/2$, then the final polarizer is needed in order to suppress the carrier. Fig. 2.2-1b shows the arrangement in which a pair of Pockels cells are employed to simulate the action of the rotating plate.

Analysis

A. Introduction.

For convenience, let us choose the +z-axis of the coordinate system along the direction of light propagation. Also, let us use a complex number representation of the x-y plane. The electric vector of a right hand circularly polarized (RHCP) ray of frequency $\omega = 2\pi c/\lambda$ will be represented, relative to a "standard" coordinate system, as

$$E_R(z,t) = Ae^{+i(\omega t - kz)} \qquad (2.2.2\text{-}1a)$$

where $k = (\omega n/c)$ and (c/n) is the velocity of light in the medium with index of refraction n.

Similarly, the electric vector of a left hand circularly polarized (LHCP) ray is:

$$E_L(r,t) = Ae^{-i(\omega t - kz)} \quad . \qquad (2.2.2\text{-}1b)$$

It can easily be verified that when such a circularly polarized ray traverses a stationary birefringent crystal which has principal axes

oriented at an angle $+\Omega$ relative to the standard coordinates, the output is: (See Appendix A)

$$E_2(z,t) = e^{\mp i\alpha} A\cos\beta + e^{\pm i[\alpha - (\pi/2) \mp 2\Omega]} A \sin\beta \qquad (2.2.2\text{-}2)$$

where the upper signs refer to RHCP and the lower signs to LHCP, $\alpha = \omega t - kz + \Omega_o$, and Ω_o is an unimportant phase angle. The retardation through the crystal is: $2\beta = (\omega/c)\, \ell\, (n_x - n_y)$.

The result is a superposition of two circularly polarized rays. The ray polarized with the same sense as the incident ray has amplitude cos β; the oppositely polarized ray has amplitude sin β and is shifted in phase by $\pi/2 \mp 2\Omega$.

B. Rotating Birefringent Crystal

The result for the RHCP of ray traversing a birefringent crystal rotating with angular velocity $+\omega_R$ follows at once by noting that the principal axes of such a rotating crystal are oriented at an angle $\Omega = \Omega_o + \omega_R t$ relative to the standard coordinate axes. The phase shift noted above becomes a frequency shift since:

$$(\alpha - \tfrac{\pi}{2} - 2\Omega) = (\omega - 2\omega_R)t - kz - 2\Omega_1 - \tfrac{\pi}{2} + \Omega_o \,. \qquad (2.2.2\text{-}3)$$

Thus, the LHCP component of the output is shifted in frequency by twice the angular velocity of rotation of the crystal.

For the case of a half wave plate, the total retardation is

$$2\beta = \frac{2\pi}{\lambda}\, \ell(n_x - n_y) = \pi \qquad (2.2.2\text{-}4)$$

so that cos $\beta = 0$ and 100% conversion of the carrier power to single sideband is obtained in the output of the rotating half wave plate. For $\beta \neq \pi/2$, a circular analyser can be employed to transmit only the LHCP component and thus completely suppress the carrier.

C. A pair of phased oscillating birefringent crystals

In Fig. 2.2-1b, the pair of KH_2PO_4 crystals are oriented with their crystallographic c-axes along the z direction. With a voltage V applied along the c-axis, the indices of refraction along the principal axes are

$$n_{x'} = n_o + \frac{1}{2} n_o^3 r \, (V/\ell)$$
$$n_{y'} = n_o - \frac{1}{2} n_o^3 r \, (V/\ell) \qquad (2.2.2\text{-}5)$$

where n_o is the ordinary index of refraction and $r = r_{63}$ is the appropriate electro-optic constant. The retardation is thus $2\beta = (2\pi n_o^3 r V/\lambda)$.

To obtain the desired effect of a rotating phase plate, we must apply a sinusoidal voltage along the c-axis of the two crystals in phase quadrature; for example, let $V_1 = V \sin \omega_m t$ and $V_2 = V \cos \omega_m t$; finally, we must introduce a spatial rotation of 45° between the principal axes of the two crystals.

In this case, the indices of refraction in the crystals are time dependent. It is necessary to examine the change in the wave equation required by a time varying index. However, for all

practical modulation frequencies, $\omega_m << \omega$, the frequency of the light wave. Therefore, it can be shown that the time derivative of the index of refraction may be neglected and the previous results for a static birefringent plate may be used.

Thus the output when a RHCP ray traverses a pair of phased, oscillating birefringent plates is obtained by applying Eq. (2.2.2-2) successively to a RHCP ray traversing the first crystal with $\Omega = 0$, and then to both a RHCP and a LHCP ray traversing the second crystal with $\Omega = +\pi/4$.

After applying many well known trignometric identities and the Bessel function expansions of $\begin{matrix}\sin\\ \cos\end{matrix}$ (A sin ωt), the output of the second crystal can be written: (see Appendix A)

$$E_3(z,t) = \frac{A}{\sqrt{2}} \sum_{n=-\infty}^{\infty} \left\{ e^{i\alpha_3} J_{2n}(\beta_o) e^{i2n\left[\omega t-(\pi/4)\right]} \left(\sqrt{2}\, e^{i\phi_n}\right) + \right.$$

$$\left. + e^{-i\alpha_3} J_{2n+1}(\beta_o)\, e^{i(2n+1)\left[\omega t+(\pi/4)\right]} \left[1 + (-1)^n\right] \right\} \qquad (2.2.2\text{-}6)$$

where $\beta_o = \sqrt{2}\,\pi n_o^3 r(V/\lambda)$, $\phi_n = (-1)^n \frac{\pi}{4}$, and $\alpha_3 = \omega t - kz - \Omega_o$ and Ω_o is an unimportant phase angle. Note that $\left[1 + (-1)^n\right] = 0$ unless n is even.

We see that the Fourier spectrum of the RHCP ray contains components with frequencies $\omega + 2n\omega_m$ and amplitudes $AJ_{2n}(\beta_o)$; whereas the LHCP ray contains frequencies $\omega - (4p + 1)\omega_m$ and amplitudes $\sqrt{2}\, J_{4p+1}(\beta_o)$, where $2p = n$ for even values of n. Finally, the circular polarization analyzer in Fig. 2.2-1 can completely suppress

the RHCP ray, which contains the carrier plus all even harmonics.

The modulation transfer characteristic is $\sqrt{2}\ J_1(\beta_o)$ which is nearly linear for β_o up to about $\pi/2$ radian. At this value the incident light power is divided as follows*: in the RHCP ray (which is suppressed) 51% at frequency ω, and 3.9% at $\omega \pm 2\omega_m$; in the LHCP ray, 45% at $\omega - \omega_m$ and 0.1% at $\omega + 3\omega_m$. In order to transmit an amplitude modulated modulating signal one must operate in the linear region. However, the maximum power which can be transferred from the carrier to the single sideband is 67% which is obtained for $\beta_o = 1.74$ radian. Pure frequency modulation of the modulating signal could equally well be transmitted at this value of β_o where the division of power is RHCP: 14% at ω, 28% at $\omega \pm 2\omega_m$; LHCP: 67% at $\omega - \omega_m$, and 1% at $\omega + 3\omega_m$. Thus 3rd harmonic distortion would be about 1.5%.

One must recognize that in practice, with available crystals, it is extremely difficult and costly in power to obtain phase retardation exceeding a few tenths of a radian in a broadband structure. Thus we are in practice limited to the linear region.

It has been recently demonstrated** that, by applying a rotating electric field to an isotropic crystal, such as ZnS, a rotating phase plate can be simulated in a single crystal. As mentioned above, this method could produce 100% power transfer to the single sideband. However, again, power limitations and the unavailability of large optically homogeneous crystals limit the power transfer to about 10% at present.

---

* Buhrer, C.F., Fowler, V.J., Bloom, L.R.; Proc. IRE, 50, 1827 (1962).

**C.F. Buhrer, D. Baird, E.M. Conwell, App. Phys. Let. 1, 46, (1962).

2.2.2.4 Production of Single Sideband Unsuppressed Carrier Optical Modulation

The transmission of the carrier along with single sideband may at times be useful in order to control the frequency of the local oscillator in heterodyne detection. The single sideband suppressed carrier optical modulator could, for instance, provide a carrier which is polarized either parallel to or orthogonal to the signal, if respectively either the final quarter-wave plate or polarizer were omitted.

Two equivalent forms of an alternative method for producing single sideband modulation with carrier are illustrated in Fig. 2.2-2. Two modulators are arranged with optical inputs that differ in phase by $\pi/2$, and with modulating inputs that are identical except that each frequency component of the modulating voltage applied to one modulator is $\pi/2$ out of phase with respect to the signal applied to the second. This technique of phase cancellation has been used extensively at R.F. frequencies and can be achieved with any form of continuous modulation*. The effect is illustrated graphically in Fig. 2.2-3.

To achieve single-sideband modulation, it is only necessary to suppress the carrier in the above system. This can be done by adding an equal part of the unmodulated carrier after a π phase change to the modulated part, by passing it through a $\pi/2$ plate.

---

*Electronic and Radio Engineering, Terman, 4th Ed. p. 541.

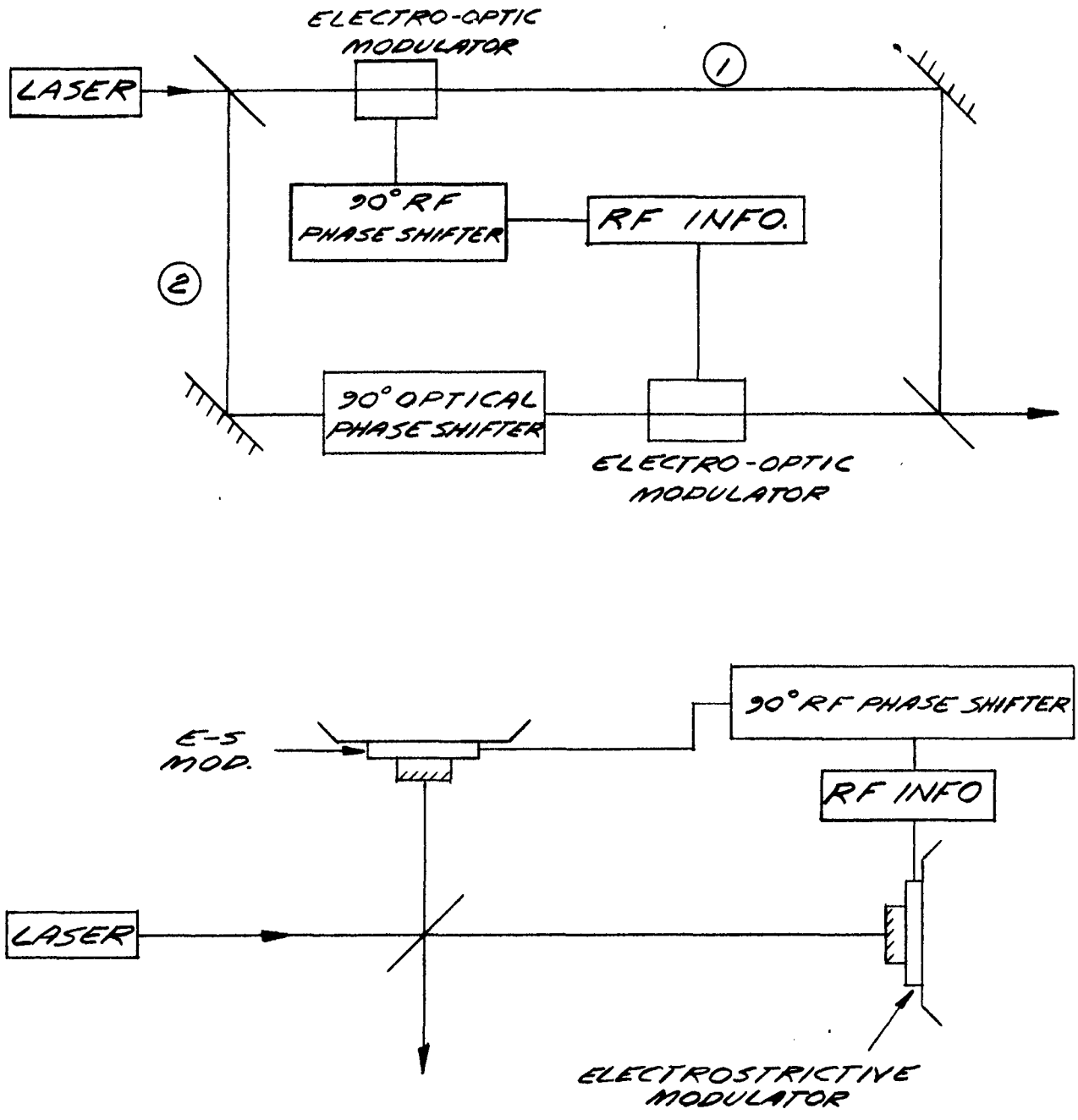

FIG. 2.2-2

TWO ARRANGEMENTS FOR PRODUCING A SINGLE SIDEBAND, UNSUPPRESSED CARRIER BEAM

FIG. 2.2-3

SINGLE SIDEBAND BY PHASE CANCELLATION

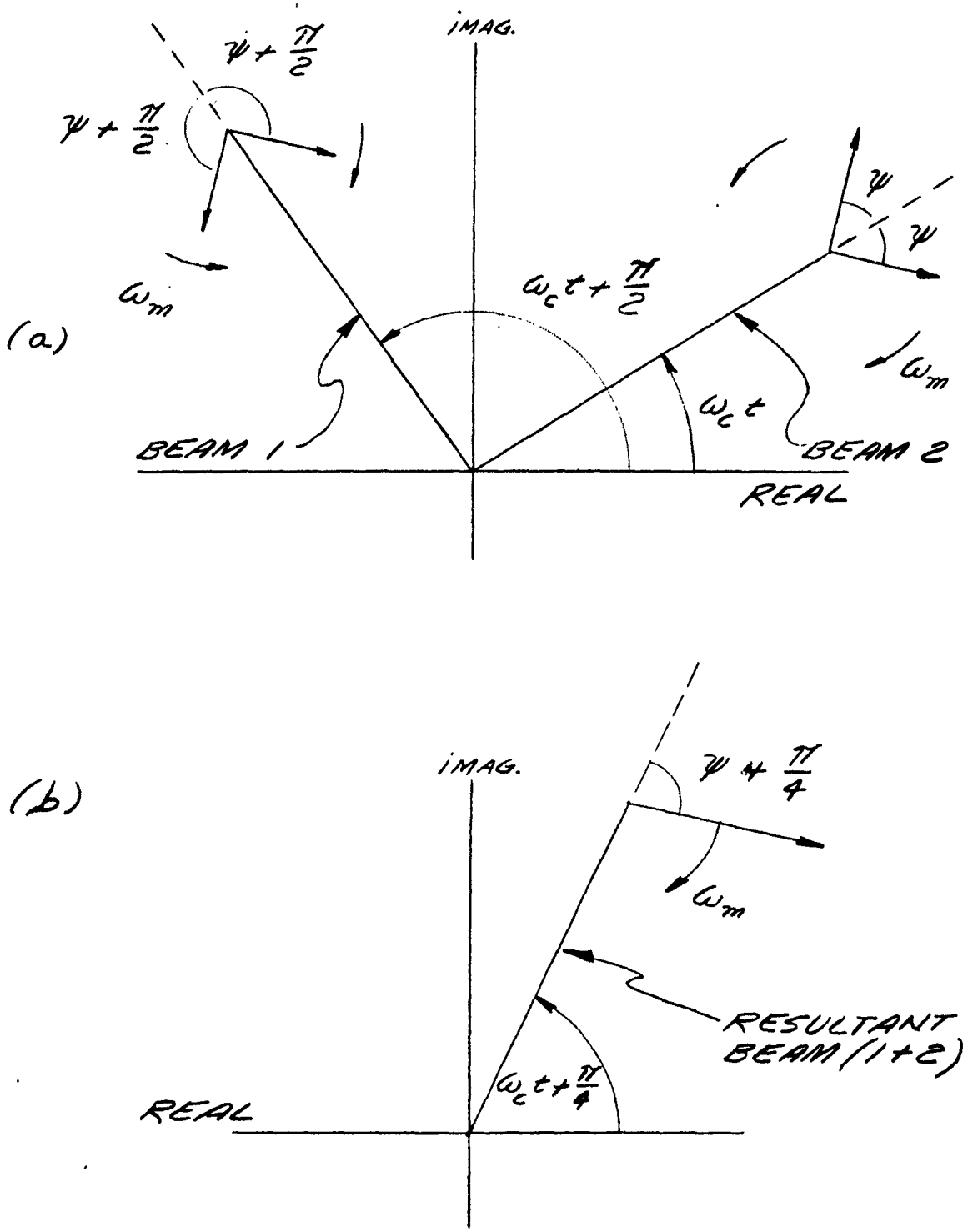

ADDING VECTORS IN (a) RESULTS IN (b) WHICH IS SINGLE SIDEBAND, UNSUPPRESSED CARRIER

The use of piezo-electric modulated mirrors to produce single sideband modulation is shown in the lower part of Fig. 2.2-2. This arrangement utilizes entirely reflective optics and mechanical modulation to circumvent the difficulties associated with transmitting a coherent beam through an optically active crystal. Such a device is readily constructed, to the highest standards of optical perfection, but it is limited to about 1 Mc in frequency response.

2.2.3 Summary of Modulators Which Presently Look Promising

A thorough investigation of modulation techniques was conducted at TRG. The results indicated that at present no light modulator is available which completely satisfies all the above criteria, although many approach them closely. The following modulators appear to best satisfy the above criteria for successful broadband optical heterodyning:

2.2.3.1 Electro-optic Effect

A. Quadratic Kerr Effect

To modulate light using the Kerr effect in isotropic liquids the direction of light propagation may be at right angles to the electric field. The plane of polarization is rotated through an angle θ given by

$$\theta = QBE^2L \qquad (2.2.3\text{-}1)$$

where $Q = \nu/\Delta\nu$, B is the Kerr constant, E is the applied field, and L is the path-length through the medium.

For broadband applications the power required per unit volume, per unit bandwidth, is

$$P = \epsilon E^2 = \frac{\epsilon\theta}{QBL} \qquad (2.2.3\text{-}2)$$

where ϵ is the permittivity of the medium. Thus, with nitrobenzene, which has the highest known B, the power/unit area, per unit bandwidth, is

$$PL_{(\theta=\pi/2)} = \frac{10^{-11}}{2B} = 2 \times 10^{-2} \text{ watts/cm}^2 - \text{cps} \; . \qquad (2.2.3\text{-}3)$$

This figure is in reasonable agreement with reported measured values. Bandwidths of the order of 3 kMc should be achievable, but so far such high frequencies have been obtained only on a pulsed basis. Thus, Holshouser* operated with a duty cycle of 10^{-4}. Heating effects would not allow cw operation.

B. Linear Kerr (Pockels) Effects in Solids.

To modulate light using the linear Kerr effect in solids, we must arrange the crystal so that the crystal axis, the direction of light propagation, and the electric field are all parallel.

---

*Holshouser, D.F., Von Foerster, H. and Clark, G.L., J.O.S.A., 51, 1360, 1961.

Upon application of an electric field the uniaxial crystal becomes biaxial, the difference in indices of refraction being

$$n_1 - n_2 = n_o^3 r_{63} E \qquad (2.2.3\text{-}4)$$

where E is the electric field, n_o is the field-free refractive index, and r_{63} is the electro-optic constant pertainant to this crystal orientation.

For a crystal L cm long, the phase shift produced is

$$\Delta\phi = \frac{2\pi}{\lambda_o} \Delta p = \frac{2\pi}{\lambda_o} L n_o^3 r_{63} E \qquad (2.2.3\text{-}5)$$

where λ_o is the vacuum wavelength of the light, Δp is the modulated path difference. If the modulator is operated so that the bandwidth is determined by the loss tangent of the material, then the power required, per unit volume, per unit bandwidth is

$$P = \epsilon E^2 = \epsilon \left[\frac{\theta \lambda_o}{2\pi L n_o^3 r_{63}} \right] . \qquad (2.2.3\text{-}6)$$

For KDP, which has one of the highest values of r_{63},
$\epsilon = 1.8 \times 10^{-12}$ F/cm, $r_{63} = 7 \times 10^{-10}$ cm/volt, $n_o = 1.47$,

$$PL_{(\theta = \pi/2)} = 2 \times 10^{-4} \text{watts/cm}^2 - \text{cps}, \qquad (2.2.3\text{-}7)$$

assuming L = 1 cm and $\lambda = 1\mu$. This value is 100 times less than that of the quadratic Kerr effect liquid nitrobenzene modulator.

In 1961, Kaminow modulated an optical beam at 9.25 kMc with an expenditure of 2×10^{-7} watts/cm^2-cps. His bandwidth was 60 Mc/sec. However, the experiment was done on a pulsed basis with a duty cycle of 1:5000. This was necessary in order to reduce the effect of heat dissipation in the crystal.

More recently, the Sperry Gyroscope Co. has developed a KDP modulator capable of continuous modulation with a 10 Mc bandwidth centered in the L-band region (1-2 kMc). The bandwidth is not limited by heating effects, but by the cavity resonance.

Several new crystals have been shown to have still higher electro-optical coefficients than KDP. Table 2.2-1 lists several of these crystals, with remarks concerning their limitations.

2.2.3.2 Faraday Rotation in Saturated Ferromagnets

This magneto-optical effect, like the electro-optical effect, introduces a differential phase lag for light polarized in different directions.

This rotation may be expressed empirically by

$$\theta = KML \qquad (2.2.3\text{-}8)$$

where K = Kundt's constant, M = magnetization per unit volume, L = pathlength through the medium.

The best material for use at 1.15μ appears to be Yttrium Iron Garnet ($Y_3Fe_5O_{12}$), for which

TABLE 2.2-1. Electro-optical coefficients of several materials

	Electro-optical coefficient	$V_{\lambda/2}$ at 5461Å	Remarks
Quartz	r_{11} = 1.4 x 10^{-8} cm/statvolt*	75 kv**	Optically active Transparent past 2.5μ.
ZnS	r_{41} = 6.4	9.3 kv	Hard to obtain; strain free
CuCl	r_{41} = 18.4	6.2	Transparent out to 15μ, but unstable in air.
$NH_4H_2PO_4$	r_{63} = -25, r_{41} = 62	9	Transparent out to 1.4μ.
KH_2PO_4	r_{63} = -32, r_{41} = 26	7.5	Transparent out to 1.4μ.
KD_2PO_4	r_{63} = 70	3.4	Transparent out to 2μ.**

* Note error in AIP Handbook.

**Private communication -- H. Jaffe.

$$\theta_{max} \text{ (optimum thickness)} = 0.6 \text{ radians} . \qquad (2.2.3\text{-}9)$$

This depth of modulation is sufficient for optical heterodyne work. However, the most serious drawback to the Faraday modulator is that the upper limit to the modulation frequency, and hence the bandwidth, is less than 10^8 cps.

2.2.3.3 Acoustical Modulation--e.g., Debye-Sears Effect

Ultrasonic waves in solids or fluids are capable of diffracting light by virtue of the periodic variation of the index of refraction accompanying the pressure variations.

A practical limit to the bandwidth of a Debye-Sears modulator may be derived by considering the propagation of a pressure amplitude step-function across the light beam diameter, d. The light intensity will then change from zero to maximum in a time of the order of d/v, where v is the acoustic velocity is less than 10^6 cm/sec. Thus we conclude, for d = 1 mm, that frequencies greater than 10 Mc are filtered out of the light response and the bandwidth can be no greater than 10^7 cps. (Commercially available Debye-Sears modulators require about 5 watts for operation over a bandwidth of 0.1 Mc.)

2.2.3.4 Piezo-electric Effect

An optically flat mirror, mounted on the face of a piezo-electric crystal may be vibrated by an alternating

electric field applied to the crystal. This will phase-modulate a light beam reflected from the mirror.

Several thousand volts are required to achieve modulation of 2π radians, at a wavelength of 1μ, but little power is absorbed by crystal hysteresis.

This technique is limited to frequencies less than 10^8 cps.

2.2.4 Newly Proposed Modulators

Because the present State-of-the-Art is not yet sufficiently advanced to meet the requirements for modulating LASERs for $\Delta\nu = 10^9$ cps, further advances should be considered.

2.2.4.1 Multipass Electro-Optic Modulators

This is a scheme for increasing the modulation efficiency obtainable from many of the above-mentioned modulators by using their capabilities to modulate the optical separation of a Fabry-Perot etalon. The effective optical separation, L, of Fabry-Perot etalon plates may be modulated either by moving the plates as described in Section 2.2.2.1 or by changing the refractive index of the medium between them. The relationship between plate separation and phase is given by

$$\phi = R \sin (2kL) / \left[1 - R \cos (2kL)\right] \qquad (2.2.4\text{-}1)$$

where $k = 2\pi/\lambda$, and R = intensity reflectance. The derivative, $\Delta\phi$, evaluated at a value of L, giving maximum transmission, is

$$\Delta\phi = \frac{2\pi}{\lambda}\left(\frac{1+R}{1-R}\right)\Delta L \quad . \qquad (2.2.4\text{-}2)$$

This is to be compared with a single pass phase retardation through a crystal given by

$$\Delta\phi = \frac{2\pi}{\lambda}\Delta L \quad . \qquad (2.2.4.3)$$

For large R, $(R \approx 1)$, the gain in phase change over the single pass case is $2/(1 - R)$. However, as was pointed out in section 2.2.2.1, the bandwidth of modulation is limited by the Q of the cavity to

$$\Delta\nu = \frac{\nu}{Q} = \frac{C}{L}\frac{(1-R)}{2\pi} \approx 1 \text{ Mc (for R = 99\%, L = 50 cm).} \qquad (2.2.4\text{-}4)$$

Thus bandwidth must be sacrificed to obtain a gain in modulation index. A serious drawback, and practical limitation to this device is the stringent requirements for optical polish, flatness, and homogeneity of the material. In effect the optical perfection of the entire modulator must be at least*

$$\frac{\lambda(1-R)}{2} \quad . \qquad (2.2.4\text{-}5)$$

---

*Born, M. and Wolf, E., "Principles of Optics", Pergamon Press, New York, 1959, p. 327 ff. For a more general discussion of Fabry-Perot modulators, see: Gordon, E.I. and Rigden, J.D., "The Fabry-Perot Electro-optic Modulator", NEREM Record, Vol. IV, 86, (1962).

2.2.4.2 Quadratic Kerr Effect With Much Reduced Cell Dimension

The modulation power required is given by

$$P = \epsilon_r E^2 V \qquad (2.2.4\text{-}6)$$

where

E is the electric field strength,

ϵ_r is the real part of the dielectric constant,

V is the volume.

In order to minimize E^2V, it has been proposed to reduce the necessary volume to the logical extreme: passing light down a fiber of active material in a single mode.

By means of this technique it is reasonable to expect a reduction in E by a factor of 10 and hence a reduction in E^2 by a factor of 100. The volume of dissipating material is also reduced.

2.3 Transmission Path

The transmission path, of course, includes whatever optical elements are required to modulate, collimate, and otherwise direct and collect the LASER beam, as well as whatever length of atmosphere is traversed in the communication system.

For single-mode transmission, the distortion caused by optical imperfections in all elements of the transmission path may degrade the S/N ratio. A discussion of the losses due to misalignment, etc., which are specific to heterodyne detection will be included in Section 2.4.3.3.

Investigations of the fluctuation in refractive index and the dispersion of the atmosphere are in progress at several other laboratories*, but results are not yet available.

2.3.1 Fluctuations in Atmospheric Refractive Index

2.3.1.1 Beam Deviation

One effect of the fluctuating regions of varying index of refraction in the atmosphere is to refract a coherent LASER beam and thus cause a change in its direction and a displacement of the beam in the plane of a receiver. Such effects can, in principal, be corrected by spatial tracking techniques. However, if regions of varying index are not large compared to the beam wave front, such refraction causes loss of coherence across the wave front which is irretrievable. Thus, for atmospheric transmission,

---

*e.g., Technical Operations, Inc., Burlington, Mass.

the LASER beam wavefront or the detector aperture must be small compared to the "coherence interval" over which such loss of coherence occurs. Several recently published results have a direct bearing on this problem.* The results indicate that, under very poor conditions, intensity variations of the order of 300 to 1 can occur over distances of 4 to 8 cm across the wave front of a well collimated light beam which has traversed 3.5 kM of turbulent air. Unfortunately the total extent of the wavefront is not given in this source. It would clearly be very difficult to operate an optical communication system of any type under such conditions.

2.3.1.2 Changes in Optical Path Lengths

In addition to the above-mentioned beam deviation due to refractive index variations, another related consequence is the change of phase caused by the change in optical path length.

Under relatively calm conditions, a 115 meter channel spectrum interference has been studied** for path lengths of 115 m, 1.5 m above ground level. The results indicate that fluctuations in the optical path difference between paths separated by an average distance of 21 cm are of the order of 100Å and have a time scale of the order of 0.01 seconds. However, it should be pointed out that the amount of wave front distortion depends on the detailed variation of index of refraction along the light path, which

---

* Straub, H.W., Session WC, Rochester Optical Society Meeting, Oct. 15, 1962.

**Erickson, K.E., JOSA 52, 781, (1962).

might be appreciably larger than the optical path difference averaged over the two path lengths.

It should be noted that the single LASER transceiver used in the present study is an excellent tool for studying such atmospheric fluctuations. Furthermore, the complementary use of a pair of frequency-stabilized LASERs, which are being studied under a parallel program, will allow an even more versatile study of atmospheric fluctuations.

2.3.2 Atmospheric Absorption

The absorption spectrum of the atmosphere is given in Fig. 2.3-1, along with the oscillation wavelengths of several interesting LASERs. It is desirable to choose a LASER wavelength which coincides with an atmospheric window of high transmission.

2.3.3 Atmospheric Dispersion

Even if it were possible to substantially eliminate the problems associated with atmospheric absorption and turbulence, there still remains the difficulty of optical dispersion which, even in perfectly isotropic optical media, tends to limit the usable information bandwidth. The frequency variation of refractive index gives rise to differences in transit time for photons of different frequency. The dispersion has not only linear frequency dependence but also higher order terms which are extremely difficult to compensate for, and which impose a bandwidth limitation.

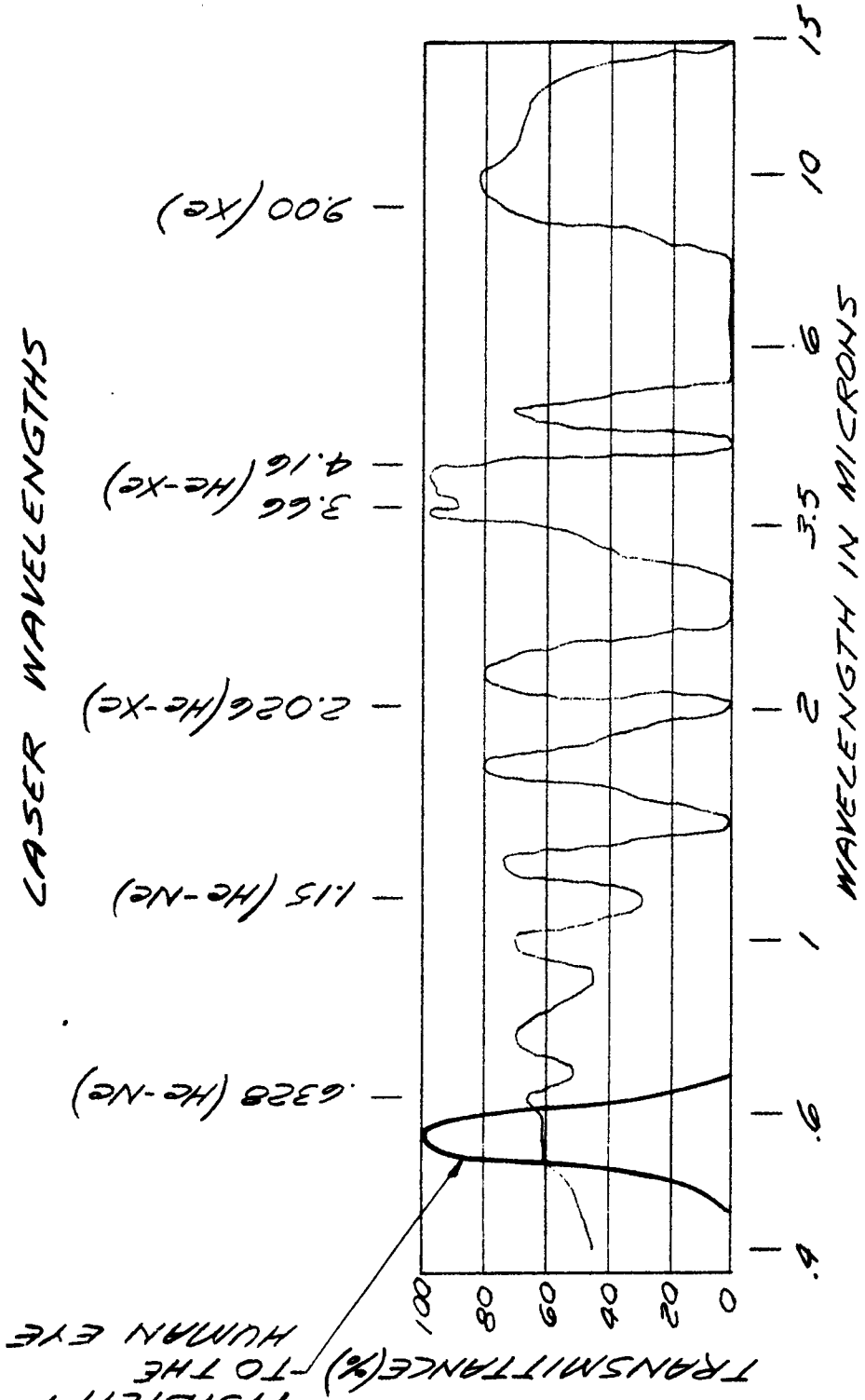

FIG. 2.3-1 TRANSMITTANCE OF THE ATMOSPHERE
2000 YD OF 17mm PRECIPITABLE WATER

A qualitative estimate of the dispersion of the atmosphere* indicates that, for bandwidths of 10^9 cycles and for transmission paths of several kilometers, the relative phase distortion in sidebands is significant. For long transmission paths, atmospheric dispersion can exceed the dispersion of the various elements of the optical system. For this reason, single sideband transmission (Section 2.2.2.3) or a detection scheme which compensates for phase distortion (Section 2.4.3.3) have been considered.

---

*Erickson, K.E., JOSA 52, 777 (1962).

2.4 Detection

2.4.1 Radiation Detectors

A beat frequency signal can only be generated by optical heterodyning in or on the surface of a detector which responde non-linearly to the radiation field. The field is the important variable, since fields add vectorially and hence interfere in time (as well as in space). Furthermore, the signal-to-noise-in-signal power ratio can be fully preserved by heterodyning on a square-law detector.

Fortunately, all sensitive radiation detectors are almost perfect square-law detectors over a wide range of frequencies and incident powers. That is, the detector-current

$$i \propto \text{incident power} \qquad (2.4.1\text{-}1)$$

or

$$i \propto \overline{\int E^2 dA}^{\tau}, \qquad (2.4.1\text{-}2)$$

the average of the square of the oscillating electric field over the photosensitive surface and over the response time, τ.

In order to make full use of the information capacity of an optical communication system, the detector must not limit either the bandwidth or the signal-to-noise ratio of the incoming LASER beam. The detector parameters of interest are the detector response time, τ, the noise-equivalent input power, NEP, the quantum efficiency, η, and the detector output resistance, R. The relative importance of these parameters must be re-examined for optical heterodyne detection.

2.4.1.1 Theoretical Considerations

In the absence of optical heterodyning, the NEP, or noise power added to the signal at the detector input, is the important parameter. Therefore, the figure of merit of a radiation detector is usually given as the detectivity,

$$D^* = \frac{\sqrt{\text{Area}}}{\text{NEP}} \quad , \tag{2.4.1-3}$$

a parameter which is independent of the detector area.

However, because of the amplification inherent in heterodyne detection, the quantum efficiency, η, supercedes the noise equivalent input power, NEP, as the fundamental figure of merit of a detector. It is shown in Section 1.3 that the shot noise-in-signal after heterodyne detection with a square-law detector is just the LASER local oscillator shot noise, which will exceed the detector dark current shot noise and Johnson noise which limits conventional detection, provided only that sufficient LASER local oscillator power is available. A large NEP merely increases the required power which must be received from the local oscillator LASER. Expressed in terms of the NEP, the requirement that the detector noise must be less than the LASER local oscillator shot noise, from Eq. (2.4.2-3), is

$$\text{NEP} \ll \left(\frac{2h\nu P_{LO}}{\eta} \right)^{1/2} \tag{2.4.1-4}$$

As an illustration, with a He-Ne LASER ($\lambda = 1.15\mu$) operating at a feeble 1 μwatt power, the requirement is

NEP $\ll 10^{-12}$ watt. If we assume that the smallest obtainable detector area is a square, 1/4mm on a side, then, in this example, we require

$$D^*(\lambda = 1.15\mu) \gg 2.5 \times 10^{10} \text{cm-watt}^{-1}\text{-cps}^{1/2} \qquad (2.4.1\text{-}5)$$

Increasing the LASER local oscillator power by a modest amount permits the use of nearly all ordinary photoconductive detectors.

On the other hand the signal-to-noise-in-signal ratio after heterodyne detection, is (Eq. 1.3-8):

$$\frac{S}{N} = \frac{\eta P}{h\nu\Delta f} \qquad (2.4.1\text{-}6)$$

Thus the S/N is degraded in proportion to the quantum efficiency η. A quantum efficiency of unity is necessary in order to make full use of the S/N available in the incoming signal. Table 2.4.1 summarizes the properties of a number of very fast and highly efficient detectors which are sensitive in the wavelength region of several promising gaseous LASERs. Figures 2.4-1 and 2.4-2 show pictorially the quantum efficiencies and detectivities of a number of radiation detectors in the wavelength region 0.3-8μ. The various types of noise which contribute to the detector NEP are discussed in Section 2.4.2.2.

2.4.1.2 Experimental Photomultiplier Study

The work to date has been limited to photoemissive detectors and to the 1.15μ He-Ne LASER. The highest photoemitter quantum efficiency available at that wavelength is that of

Table 2.4-1

Detectors Suitable for Opticel Heterodyning with Various LASERs

LASER	λ	Detector	Operating Temp.	R ohms	D*(λ) cm/sec-cps$^{1/2}$	τ sec	η
He-Ne	0.6328μ	S-20 (photomultiplier)	300°K	$\sim 10^{14}$ (1) $\sim 10^{7}$	10^{15}	$\lesssim 10^{-10}$ (2) $\sim 10^{-9}$ (3)	.05
		silicon (photovoltaic)	300°K	10^{6}	3×10^{12}	$\sim 10^{-8}$ (4)	>.9 (5)
He-Ne	1.15μ	S-1 (photomultiplier)	300°K	$\sim 10^{14}$ (1) $\sim 10^{7}$	10^{11} (6)	$\lesssim 10^{-10}$ (2) $\sim 10^{-9}$ (3)	.0001
He-Ne	1.15μ	Ge (photovoltaic)	300°K	10^{3}	10^{11}	$\sim 10^{-8}$ (4)	>.9 (5)
Cs-He	3.20μ	InAs (photovoltaic)	195°K	10^{3}	10^{12}	$\sim 10^{-8}$	>.9 (5)
He-Xe	2.06μ						
He-Ne	3.39μ	InSb (photovoltaic)	77°K	10^{4}	5×10^{10}	$\sim 10^{-8}$	>.9 (5)
Cs-He	7.18μ	Ge(Au) (photoconductive)	77°K	10^{6}	5×10^{9}	$\sim 10^{-7}$	.2

(1) Effective Johnson noise cathode resistance of multiplier is M^2R(anode) where M is current gain. See Section 2.4.2.2.

(2) Response time of the photo emitter is $\lesssim 10^{-10}$ sec.

(3) Response time of the photomultiplier is $\sim 10^{-9}$ sec.

(4) Response time is limited by RC time constant.

(5) Additional loss of .3 is incurred due to Fresnel reflection. This could, in principle, be eliminated.

(6) Noise can be reduced two orders of magnitude upon cooling.

FIG. 2.4-1

QUANTUM EFFICIENCY OF SEVERAL RADIATION DETECTORS AS A FUNCTION OF WAVELENGTH

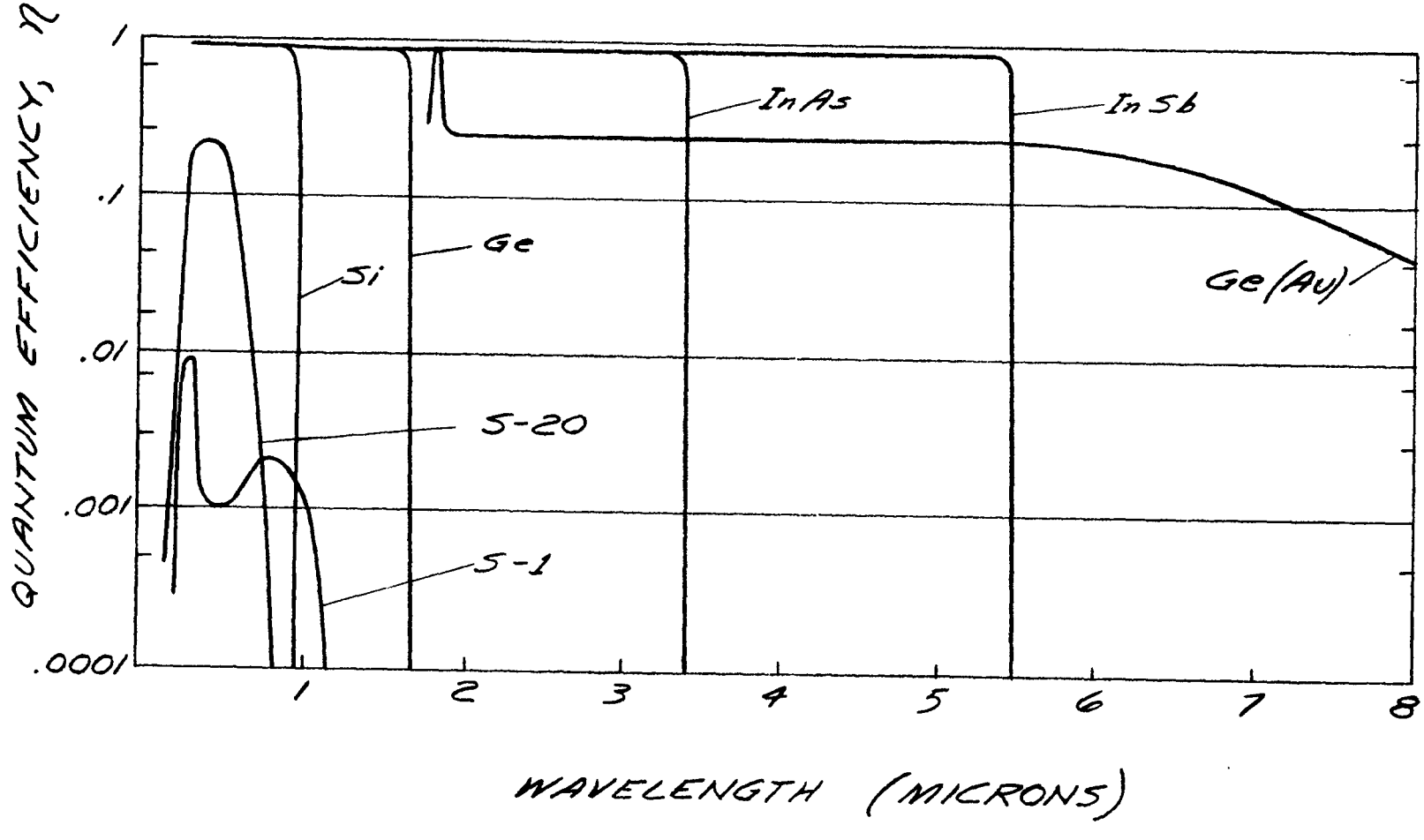

FIG. 2.4-2

SPECTRAL SENSITIVITY OF SEVERAL RADIATION DETECTORS

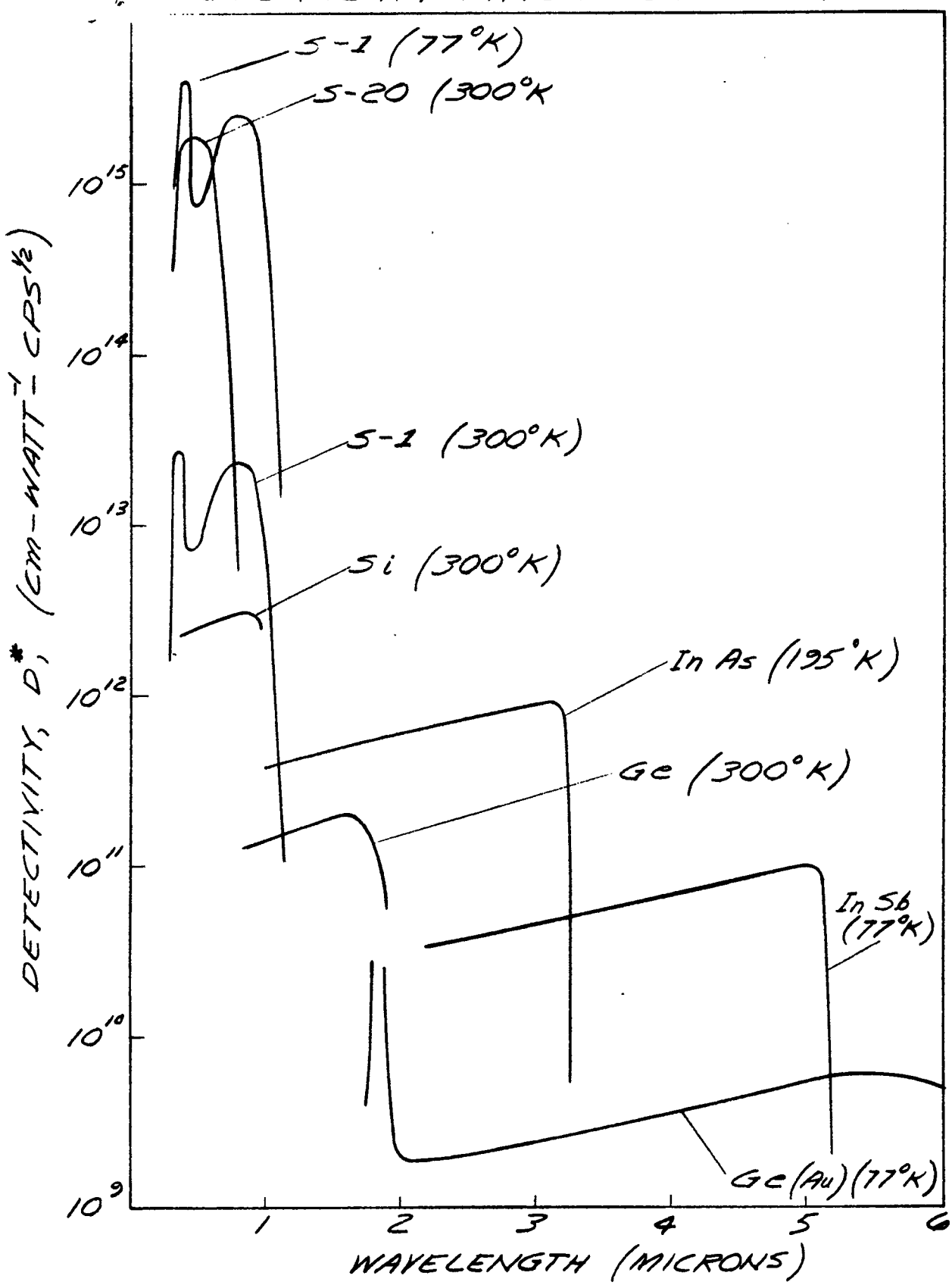

the S-1 surface whose spectral sensitivity and quantum efficiency are shown in Fig. 2.4-3.

The first step in our experimental work on detectors was the calibration of eleven S-1 photomultipliers at $\lambda = 1.15\mu$ and a study of their detection properties. The S-1 photomultipliers studied were of two types: RCA 7102 and Dumont 6911. Of these, three RCA tubes were found to be unreliable while all three Dumont tubes had such low quantum efficiencies that they were not used for further LASER noise studies.

Table 2.4-2 summarizes the measurements of photomultiplier properties. The measurements were made by irradiating the photomultiplier with a He-Ne LASER beam. The incident power level was maintained in the neighborhood of 1 milliwatt, as measured by an Epply thermopile. Optical attenuators were inserted into the beam to keep the anode current always below the rated levels (10μa for RCA 7102; 1 ma for Dumont 6911). Quantum efficiency was determined by measuring the current at the first dynode with all other dynodes and anode at cathode potential. The cathode current is not critically dependent upon potential difference between cathode and dynode No. 1.

2.4.2 Noise

The best detector is that which adds minimum noise to the incoming signal and therefore can process information at the greatest rate. The generation of noise in detectors is analyzed below with this criterion in view.

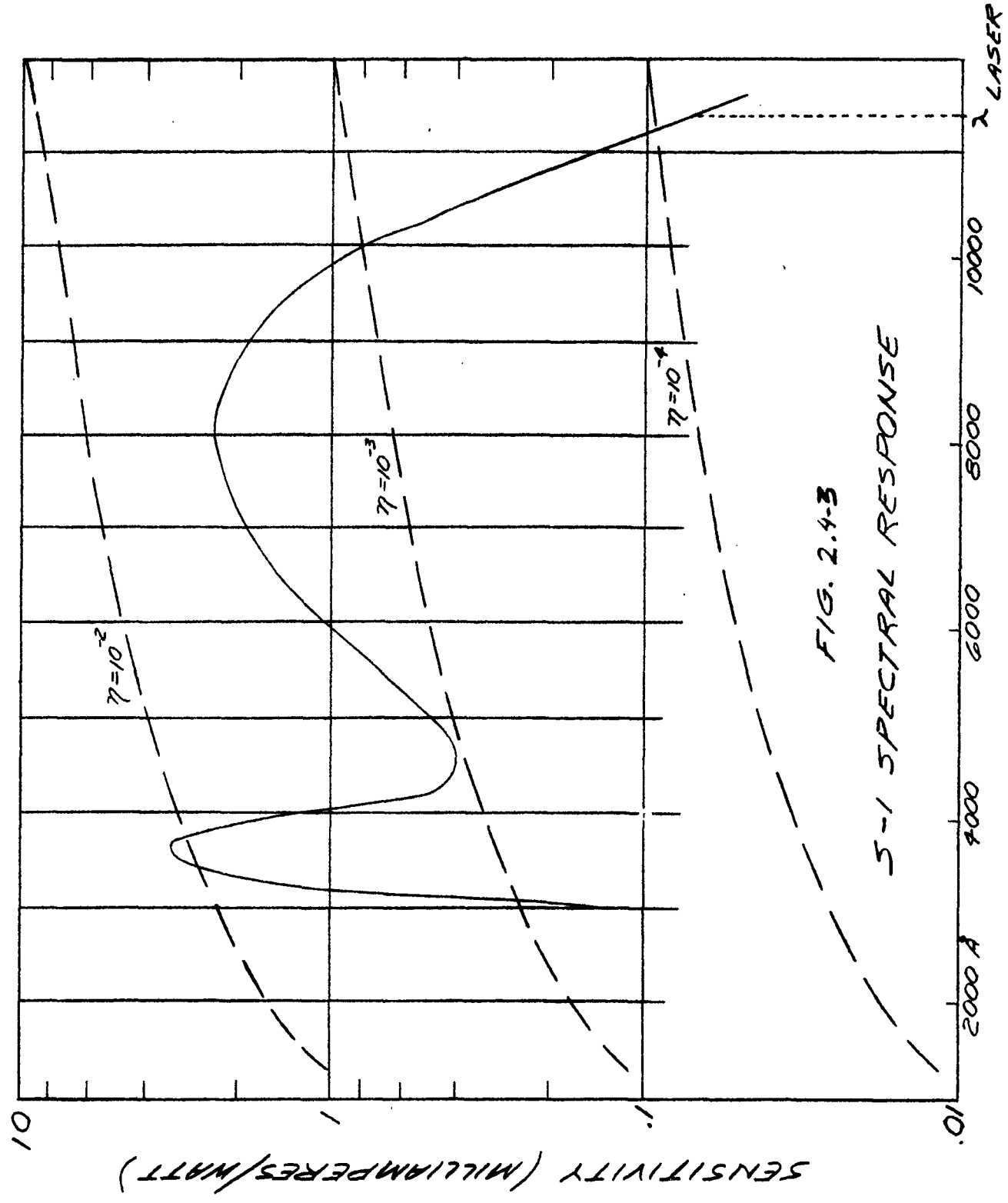
λ LASER
10000
8000
6000
4000
2000 Å
10
1
.1
.01
SENSITIVITY (MILLIAMPERES/WATT)
η=10⁻²
η=10⁻³
η=10⁻⁴
S-1 SPECTRAL RESPONSE

FIG. 2.4-3

Table 2.4-2

Detection Properties of Some S-1 Photomultipliers at $\lambda = 11530\text{Å}$

Tube	Dark Current (amp)	Quantum Efficiency (electron/photon)	Responsivity (amp/watt)	Gain (at 1200 v)	Remarks
7102 #1	1.3×10^{-8}	1.6×10^{-5}	.33	8×10^{3}	Unreliable. Loose internal connection
#2	3.2×10^{-6}	1.9×10^{-4}	20	1.3×10^{5}	High responsivity, high noise
#3	8×10^{-8}	2.3×10^{-5}	1.0	6×10^{4}	
#4	4×10^{-9}	7×10^{-6}	.13	2.5×10^{4}	
#5	4×10^{-7}	4.4×10^{-5}	3.4	9×10^{4}	
#6	4×10^{-9}	2.7×10^{-5}	.008	3×10^{4}	Unreliable. Loose internal connection
#7	2.5×10^{-6}	3.5×10^{-5}	8	3×10^{5}	
#8	2×10^{-6}	2.5×10^{-5}	9	5×10^{5}	
6911 #1	1×10^{-8}	11×10^{-7}	.07	8×10^{5}	
#2	6×10^{-9}	9×10^{-7}	.24	3.2×10^{5}	
#3	2.5×10^{-7}	8×10^{-6}	.13	2×10^{4}	

In this discussion, it will be convenient to express the LASER beam power, P, and the photon-generated current in the detector, i, in terms of the flow of photons (of energy, $h\nu$,) and electrons (of charge, e):

$$\frac{i}{e} = \eta \frac{P}{h\nu} = \eta n \qquad (2.4.2\text{-}1)$$

where η is the quantum efficiency, or the number of photo electrons generated per photon, and n is the number of photons arriving at the detector per second.

2.4.2.1 Noise-in-Signal of a LASER Beam

The irreducible "noise-in-signal" in any light beam is due to the statistical fluctuations in the finite photon flux in the beam. This noise has been called "radiation shot noise".*

$$\overline{(\Delta n)^2} = 2(\text{no. of photons/sec})\Delta f \qquad (2.4.2\text{-}2)$$

or

$$\overline{(\Delta P)^2} = 2(h\nu)P_{av}\Delta f \qquad (2.4.2\text{-}3)$$

That is, the mean square power fluctuations is proportional to the bandwidth, Δf, and $\overline{\Delta P^2}$ is the proper bandwidth proportional noise parameter. Expressing the signal in the same form, we obtain

---

*R. Clark Jones, Proc. Inst. Rad. Eng. 47, 1481 (1959).

$$S/N = P_s^2/2(h\nu)P_{av}\Delta f \qquad (2.4.2\text{-}4)$$

Let the signal radiation power, $P_s = P_{av}$. Then

$$(S/N)_{max} = \frac{P}{2h\nu\Delta f} = \frac{1}{2\Delta f} \text{ (no. of photons/sec)} \qquad (2.4.2\text{-}5)$$

Eq. (2.4.2-5) does not give the correct maximum signal-to-unit-bandwidth noise ratio at all frequencies. Additional fluctuations occur because of the statistical properties of photons. However, the power spectrum*,** of the added fluctuations is confined to the frequency range $0 < \nu < 2\Delta\nu$ where $\Delta\nu$ is the full frequency width at half intensity of the light beam. The complete noise spectrum is graphically illustrated in Fig. 2.4-4. Since for a LASER, $\Delta\nu$ is less than a few cycles per second (see Section 2.4.3.3) this noise can be neglected for all practical cases where communication bands will be at higher frequencies.

Even in the absence of background or detector noise, the above S/N will not be achieved in a photo detector because of quantum inefficiencies. The mean square shot fluctuation in the current of electrons of finite charge, e, from the photo-detector is

---

* E.M. Purcell, Nature, 178, 1449 (1956).

** Lawson, J.L. and Uhlenbeck, G.E., "Threshold Signals", p. 69 (McGraw Hill, 1956).

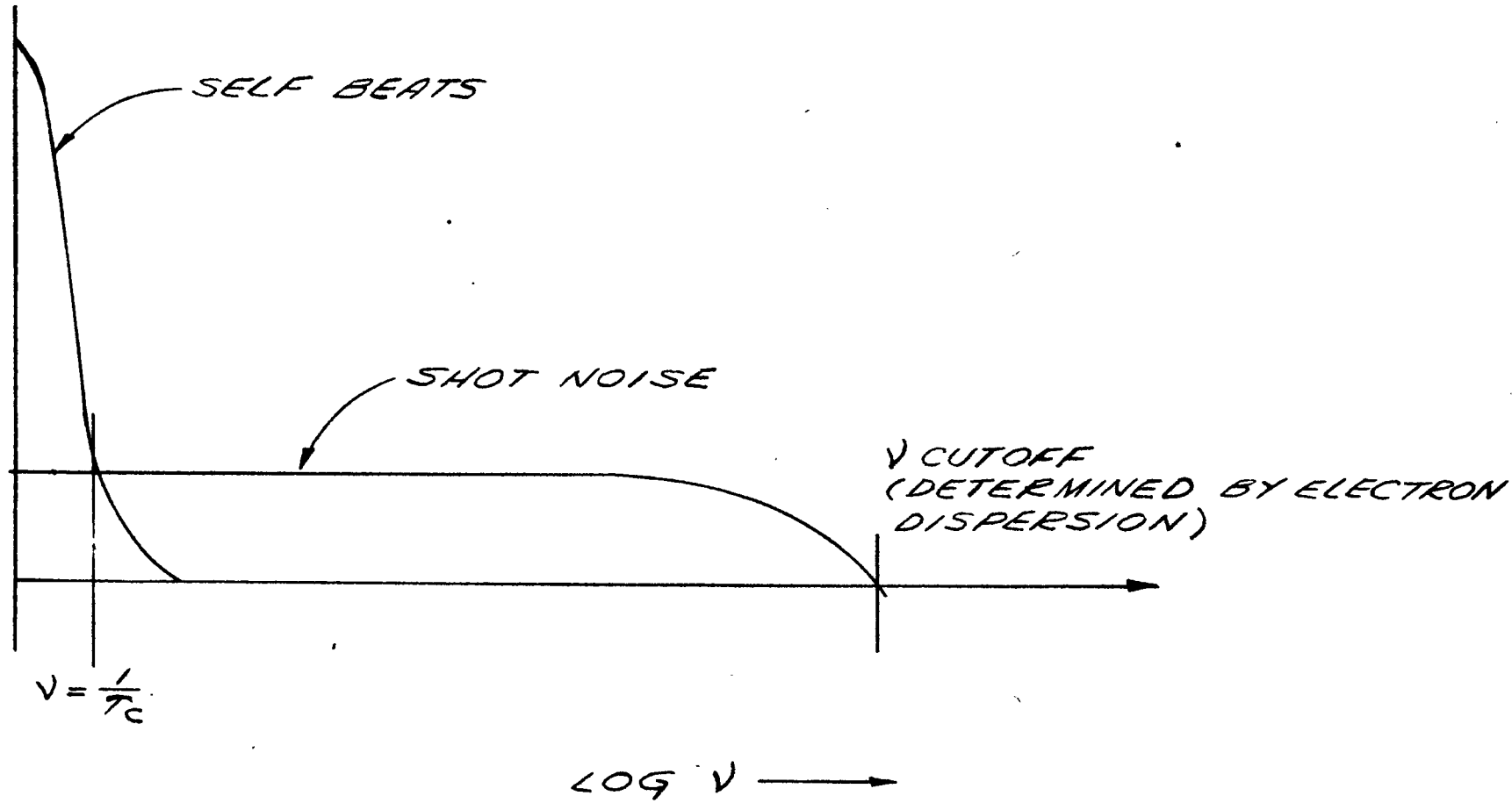

PHOTO TUBE NOISE POWER SPECTRUM

FIGURE 2.1-4

given by

$$\overline{(\Delta i)^2} = 2ei\Delta f \ . \qquad (2.4.2\text{-}6)$$

Assume, for the moment, that the current, i, is due only to signal. Again, the signal must be expressed in the same form as the bandwidth-proportional noise parameter: $S = i^2$, Therefore

$$S/N = \frac{i}{2e} = \frac{1}{2} \text{ (no. of cathode electrons per sec)}\Delta\nu \qquad (2.4.2\text{-}7)$$

But from Eq. (2.4.2-1),

$$S/N = \frac{\eta}{2} \text{ (no. of incident photons per sec)}\Delta\nu \ . \qquad (2.4.2\text{-}8)$$

Thus the statistical fluctuation in the rate of generation of photo electrons corresponds to the random absorption of individual photons. For a quantum conversion efficiency, $\eta = 1$, S/N in the photocurrent is the same as the radiation noise.

2.4.2.2 Noise Other Than Noise-in-Signal

In general a current independent of the signal current will flow from the cathode (e.g., the thermionic "Dark current"). The mean square shot fluctuations in this current, given by Eq. (2.4.2-6) will reduce the signal-to-noise ratio unless

$$i_s = i_{signal} >> i_{zero\text{-}signal} = i_o \ , \qquad (2.4.2\text{-}9)$$

since the ratio of signal-to-shot-noise in the output of the photo-detector is now given by

$$S/N = \frac{i_s^2}{2e(i_o + i_s)\Delta f} = \frac{i_s}{i_o + i_s}\,\eta(S/N)_{optimum} \cdot \qquad (2.4.2\text{-}10)$$

That is, the communication rate is directly reduced by the ratio of signal current to zero-signal or background current. The quantity $Q_D = \eta(i_s/i_o)$ has been called the "Detective Quantum Efficiency".*

Any source of noise which is proportional to the amplification bandwidth may be expressed as the shot fluctuations of an equivalent D.C. zero-signal current or photon flux. In optical communication this category includes all important types with the possible exception of purposeful jamming. The currents leading to fluctuations equivalent to various noise sources are calculated below.

A. Dark Current. Experiment has shown** that the fluctuations in the "Dark Current" are characteristic of temperature-limited thermal emission of electrons:

$$\frac{\overline{\delta(\Delta i)^2}}{\delta f} = 2ei\left\{1 + \frac{F}{f}\cdot\frac{i}{A}\right\} \qquad (2.4.2\text{-}11)$$

---

* R. Clark Jones, loc. cit.

** Ibid. Also see, "Dumont Photomultiplier Phototubes" (Dumont Industrial Tube Sales Dept., Clifton, N.J., 2nd Ed., 1959).

where the first term is "shot" noise and the second is "flicker" or "1/f" noise. The latter becomes small when f > 1 to 100 cps, and can be eliminated by using communication bands at higher frequency.

The amount of the dark current is proportional to the cathode area. The minimum cathode area may be determined by the maximum permissible light intensity on the cathode. Since the dark currents are usually smaller than that due to background light the cathode area need not be inconveniently small.

B. Background Light. The signal is transmitted against a broad background of incoherent light which generates a zero-signal current. The fluctuations in this current are just the shot fluctuations.*

By an elementary derivation, the total background light power intercepted by the photo-detector is

$$P_b = \frac{\pi I_{b\Omega}}{4F^2} A_{det} \qquad (2.4.2\text{-}12)$$

where

$I_{b\Omega}$ = angular brightness of the filtered background source in beam direction

= $\frac{\text{Power}}{\pi \text{ Area}}$ for a surface obeying Lambert's law

A_{det} = detector area

F = $\frac{\text{focal length}}{\text{diameter}}$ = "F-number" of light gathering system.

---

*These photons are statistically independent in the spectral region where the photon energy, $h\nu > KT$, where T = black-body temperature of the source of background radiation. Such is the case for visible photons from all natural sources, (e.g., the sun).

Now for any expected communication distance, the signal will arrive as a plane wave to be focussed on the photo-detector, or on a pinhole in an opaque screen. The "coherence area" of the central Fraunhofer diffraction spot, containing the bulk of the intercepted signal is:

$$\text{Effective Fraunhofer Area} = \frac{4}{\pi}(F\lambda)^2 \qquad (2.4.2\text{-}13)$$

The area which intercepts background light must be larger by a factor, $\zeta^2 > 1$, sufficient to allow tracking and/or acquisitions of the signal beam by scanning. The minimum value of the intercepted background light is thus independent of the "F"-number or any other parameter of the light-gathering lens system. It is, from Equations (2.4.2-12 and -13),

$$P_b = I_{b\Omega}\zeta^2\lambda^2 \qquad (2.4.2\text{-}14)$$

The brightness of possible background sources varies from that of the sun to that of sunlight reflected from the earth, moon, planets or scattered by the atmosphere. This light can be filtered by means of multilayer interference filters to a $\Delta\lambda = 10\text{Å}$ minimum bandwidth in the neighborhood of the LASER wavelengths; for an example, take $\lambda = 6328\text{Å}$. In principle, the light could be further filtered to a 1Å bandwidth by means of multiple birefringent filters. However, such narrow bandwidth birefringent filters are rather temperature-sensitive and probably impractical.

Representative minimum values of zero-signal photon flux at the detector due to various backgrounds are given in Table 2.4-3.

C. Thermal or "Johnson" Noise. Thermal noise is generated in the output resistance of the photodetector. The thermal noise power is given by the Nyquist formula* as

$$P_N = N_o(\text{thermal}) = 4kT\Delta f \qquad (2.4.2\text{-}15)$$

The use of a many-stage electron multiplier greatly reduces, but does not eliminate, the Johnson noise relative to shot noise. The multiplier is a current transformer. The mean square thermal noise current at the anode resistance is

$$\overline{i^2_{\text{thermal}}} = \frac{4kT\Delta f}{R_{\text{anode}}} \qquad (2.4.2\text{-}16)$$

If we equate this to the multiplied shot fluctuation of an average cathode current, we see from Eq. (2.4.2-6) that

$$\frac{4kT}{R_{\text{anode}}} = M^2(2ei_o) \qquad (2.4.2\text{-}17)$$

or

$$i_{o(\text{thermal})} = \frac{2kT}{eM^2R_{\text{anode}}} = \frac{0.05 \text{ volts}}{M^2R_{\text{anode}}} \qquad (2.4.2\text{-}18)$$

---

*R. Clark Jones, loc. cit.

TABLE 2.4-3 OPTICAL BACKGROUNDS

SOURCE	BRIGHTNESS	FILTERED BRIGHTNESS	MINIMUM DETECTOR FLUX
	I_b in watts/cm^2	I_b in watts/cm^2 with $\Delta\lambda$ = 10Å, λ = 6000Å	P_b in photons/sec from Eq. (2.4.2-12) with ζ^2 = 10 Fraunhofer modes, $\lambda = 5 \times 10^{-5}$ cm
Sun	6200 watts/cm^2	8 watts/cm^2	2.5×10^{12} photons/sec
Earth, Moon	0.14	$\sim 10^{-4}$	3×10^{7}
Daylight Sky	0.01	$\sim 10^{-5}$	3×10^{6}

where

M = multiplier current gain, assumed noiseless

$M^2 R_{anode} = R_n$ = equivalent cathode noise resistance (which is to be compared with the output resistance in the case of a photo conductive detector) in ohms.

$i_o(\text{thermal})$ = that photocurrent which would generate shot noise equivalent to Johnson noise in the output resistance.

Alternatively, note that the Johnson noise is equivalent to the shot fluctuations in a photon current:

$$n_{o(\text{thermal})} = \frac{i_{o(\text{thermal})}}{\eta e} = \frac{1}{\eta M^2 R_a} 3 \times 10^{17} \text{photons/sec.} \qquad (2.4.2\text{-}19)$$

or a beam power of

$$P_{o(\text{thermal})} = \frac{h\nu \cdot 2kT}{\eta M^2 R_a} = \frac{6 \text{ milliwatt}}{\lambda \eta M^2 R_a} \qquad (2.4.2\text{-}20)$$

when the wavelength, λ, is expressed in microns.

The latter expressions indicate the significance of Johnson noise and emphasize the advantage of internal amplification when directly detecting a signal. The internal amplification can raise the signal above the level of the Johnson noise in a relatively small output resistance which is compatible with broadband detection.

Photomultiplier detectors of conventional design cannot respond to frequencies in excess of $\nu \approx 10^8$ cycles/sec due to

electron dispersion. The emission time of a photoelectron is known to be 10^{-10} sec. High frequency photomultipliers have been designed*,** with improved frequency response. An even broader bandwidth is possible with the Travelling Wave Phototube*** which has covered the frequency range of 2 to 4 Gc/sec.

However, heterodyne detection reduces the need for post amplification. For example, from Eq. (2.4.2-20) with unit quantum efficiency ($\eta = 1$), the shot noise on the photocurrent generated by even a 1μwatt LASER at 1.15μ will exceed the Johnson noise without post multiplication ($M = 1$) if $R = 6000\Omega$.

2.4.2.3 Experimental Investigation of S/N

The theoretical dependence of the S/N on a LASER beam has been investigated experimentally. The calibration of the photomultipliers is described in Section 2.4.1.

The signal-to-noise in detection of the LASER beam was measured, using attenuators to progressively attenuate the LASER beam and a photomultiplier plus oscilloscope to observe the S/N. The incident power level was measured with an Eppley thermopile. The effective bandwidth, Δf, of phototube + cable + C.R.O. was determined by measuring that circuit's time constant; the quantum efficiencies of the various photomultipliers were measured, as previously discussed.

---

* Morton, G.A. et al, IRE Trans. Nucl. Sci. NS-5, 98 (1958).
** Gaddy, O.L. and Holshouser, D.F., Proc. IRE 50, 207 (1962).
*** e.g., Lucy, R.F., NEREM Record 1962, p. 92.

Fig. 2.4-5 shows a comparison between the theoretical LASER noise-to-signal voltage ratio

$$\frac{\Delta P}{P} = \sqrt{\frac{2h\nu\Delta f}{\eta P}}$$

and the noise-to-signal ratio as measured on the screen of a C.R.O.,

$$\sqrt{\frac{\overline{\Delta i^2}}{i}} \quad .$$

The points, corresponding to various phototubes and various incident power levels, lie close to a straight line whose slope is 15% less than 45°. (The 45° line represents a one-to-one correspondence between the theoretical and experimental quantities.) The 15% systematic deviation is probably due to the subjective nature of the determination of the noise envelope on the C.R.O. screen.

Measurements of the noise power spectrum have also been made in the frequency band between 10 cycles and 23 Mc. This was effected in the range between 10 cycles and 50 kc with an R.M.S.-reading audio spectrum analyzer having a bandwidth of 6 cycles. The noise spectrum was found to be white in this band, and agreed quantitatively with the measurements made with the C.R.O. In the region 50 kc-23 Mc, a C.R.T. spectrum analyzer was employed and the noise was found to be white out to 23 Mc within an experimental accuracy of $\pm$ 30%. Measurements to higher frequencies were not made since it was found that, with the available spectrum analyzer, instrument noise was comparable with the LASER noise, making any measurements in this region unreliable.

FIG. 2.4-5

MEASURED VS. THEORETICAL
LASER NOISE-TO-SIGNAL RATIO

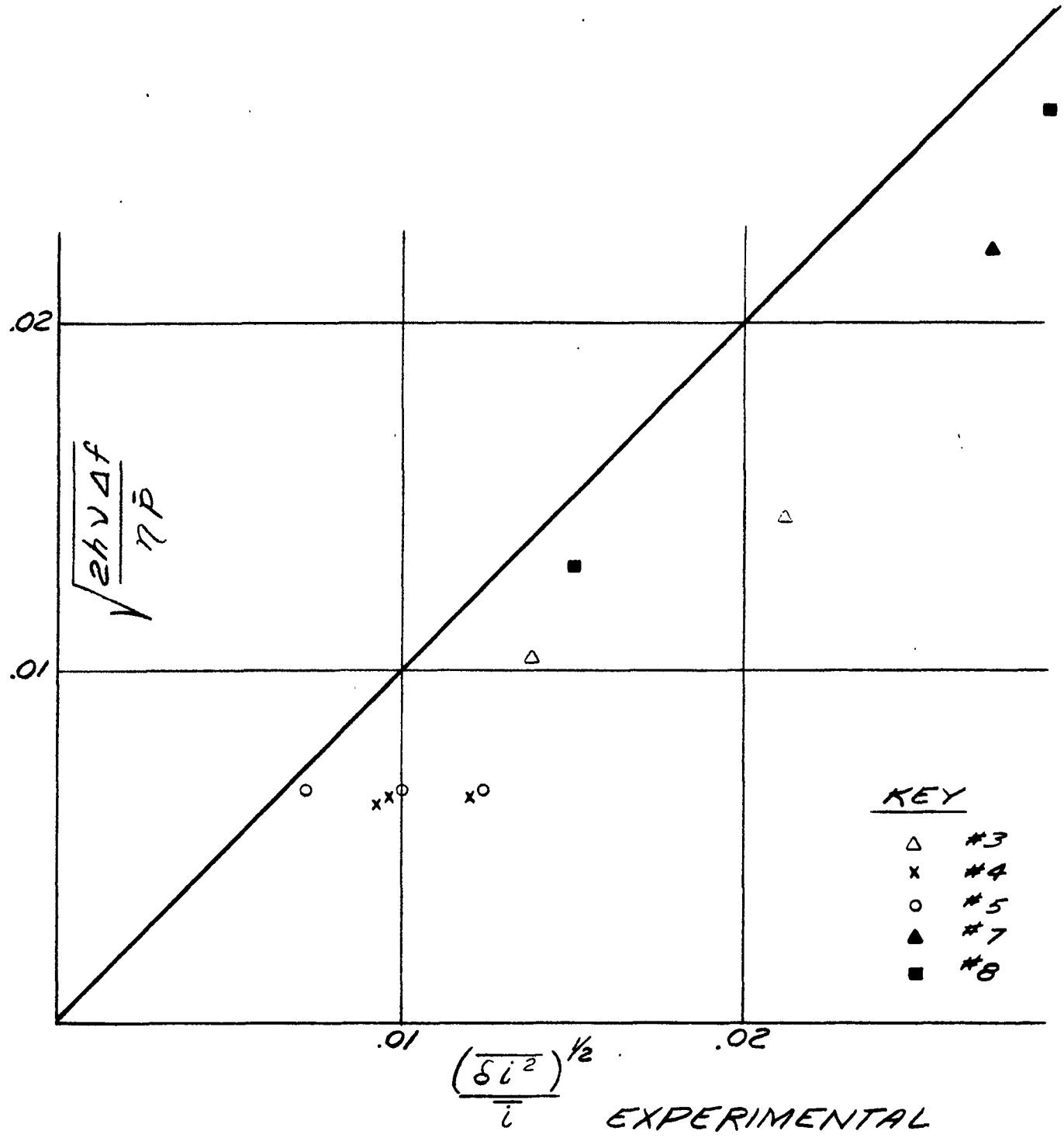

2.4.3 Optical Heterodyne Detection

The purpose of the present program is to establish experimentally the remarkable theoretical expectation that, by heterodyning with a strong local oscillator, the ratio of signal-to-noise-in-signal will be preserved in the face of large, fluctuating background and/or instrumental noise.

As is explained in the Introduction, the present experimental work on optical heterodyne detection is confined to arrangements where a single LASER is used as a source for both signal and local oscillator beams. In this way the problems of LASER stabilization and frequency-locking may be temporarily postponed while the principle of broadband heterodyning is verified.

In general, heterodyne detection is performed with a finite frequency difference between the local oscillator and the incoming signal. Homodyne detection is a special case in which a zero frequency offset is employed.

For future reference, note that in the following section, in Eq. 2.4.3-1, the term

$$\frac{m}{2}\left(e^{-i\omega_m t} + e^{i\omega_m t}\right) = m \cos \omega_m t$$

represents one Fourier component of the informationbband frequency spectrum. In general in order to avoid low frequency noise and also for purposes of multiplexing several channels on one optical carrier, each information channel will be transmitted on a subcarrier. In such a case one can let ω_m be the subcarrier frequency and let

$$m = m_o(1 + k \cos \omega_k t)$$

where $k \cos \omega_k t$ represents one component of the information band Fourier spectrum. In such cases, the information will be retrieved by following the optical detector with a second detector at the carrier frequency.

2.4.3.1 Analysis of Homodyne Demodulation

The experimental arrangement which is employed for homodyne detection is shown in Fig. 2.4-6. A beamsplitter is used to split the LASER output beam into two spatially distinct beams whose relative phases and amplitudes may be independently altered.

An optical homodyne detection system has certain unique advantages in demodulation that make it an extremely attractive and simple system for optical transmission and detection. In particular, such a system, operating with an optical square-law detector, directly demodulates phase or frequency modulation without the use of an optical discriminator. It also demodulates any mixed modulation of A.M. and P.M. without loss of information.* Optical discriminators have been proposed**, but are technologically awkward in their use.

---

* This technique of demodulation was first suggested for use at R.F. frequencies by M.G. Crosby, Proc. IRE, p. 126, Feb. 1939.

** Harris, S.E. and Siegman, A.E., "A proposed FM phototube for demodulating microwave-frequency-modulated light signals", IRE Trans. on Electron Devices, vol. ED-9, pp. 322-329; July, 1962.

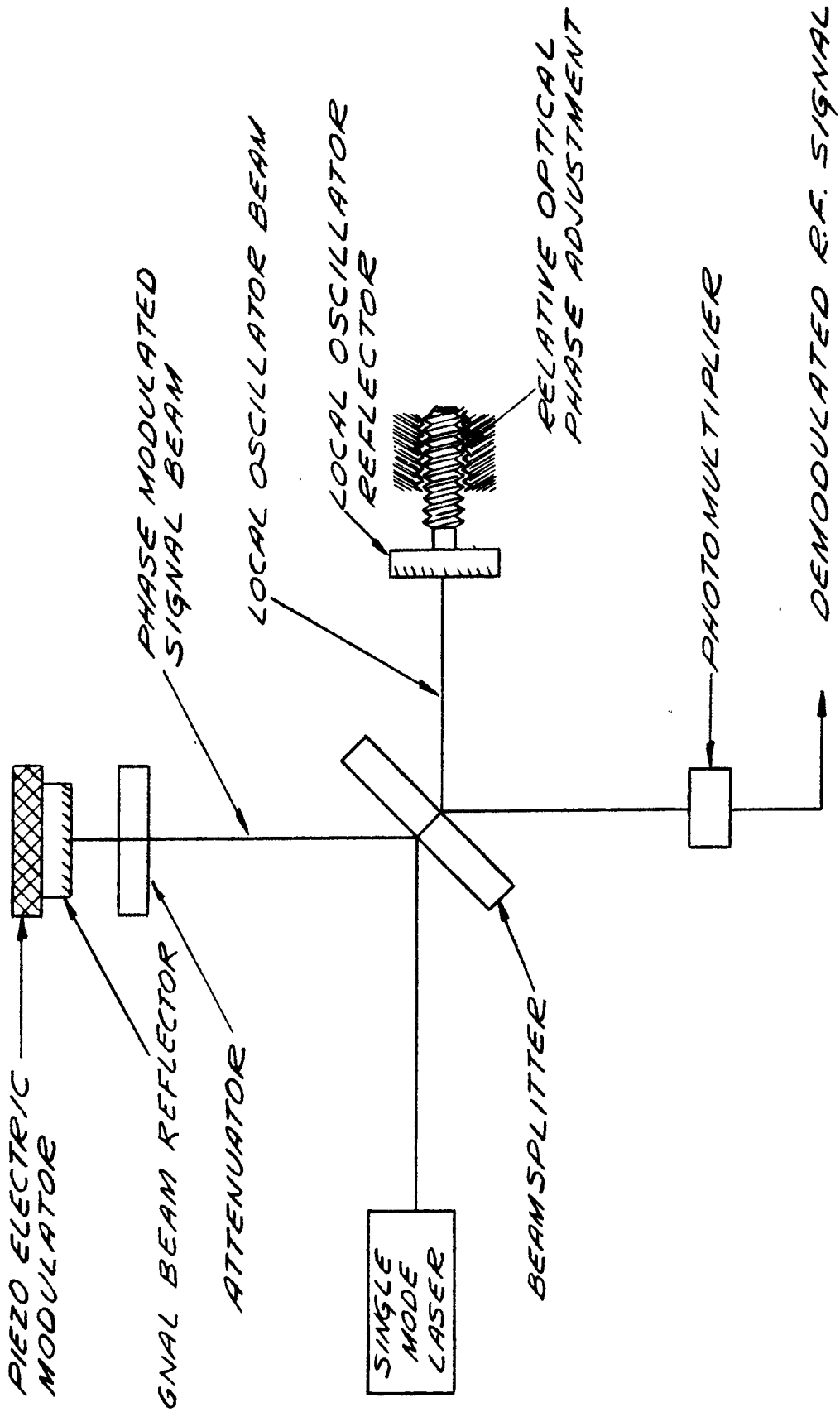

FIG. 2.4-6

OPTICAL HOMODYNE DETECTOR

Demodulation is achieved* simply by adjusting the relative phase of the optical carrier and local oscillator. A graphic illustration of a mixed modulation is shown in Fig. 2.4-7, where, for a single polarization,

$$E_L e^{i(\omega t + \phi)}$$

represents the magnitude and phase (with respect to the carrier) of the local oscillator of angular frequency ω and

$$E_c \left\{ e^{i\omega t} + \left(\frac{m}{2}\right) e^{i\left[(\omega - \omega_m)t + \psi\right]} + \left(\frac{m}{2}\right) e^{i\left[(\omega + \omega_m)t + \psi\right]} \right\} \qquad (2.4.3\text{-}1)$$

represents the optical carrier plus sidebands; here

m = modulation index,

ω_m = modulator angular frequency,

ψ = phase of the modulation sidebands with respect to the carrier.

If $\psi = 0$ or π, modulation is purely in the amplitude. If $\psi = \pm \pi/2$, modulation is purely in the phase. With an arbitrary ψ, modulation is mixed.

The resultant field at the square-law detector is

$$\mathcal{E}_R = \mathrm{Re} \left\{ E_L e^{i(\omega t + \phi)} + E_c e^{i\omega t} + E_c \left(\frac{m}{2}\right) e^{i\left[(\omega - \omega_m)t + \psi\right]} + E_c \left(\frac{m}{2}\right) e^{i\left[(\omega + \omega_m)t + \psi\right]} \right\} \qquad (2.4.3\text{-}2)$$

---

*Rabinowitz, P., Jacobs, S., Targ, R., Gould, G., "Homodyne Detection of Phase-modulated Light", Proc. IRE, vol. 50, p. 2365, Nov. 1962.

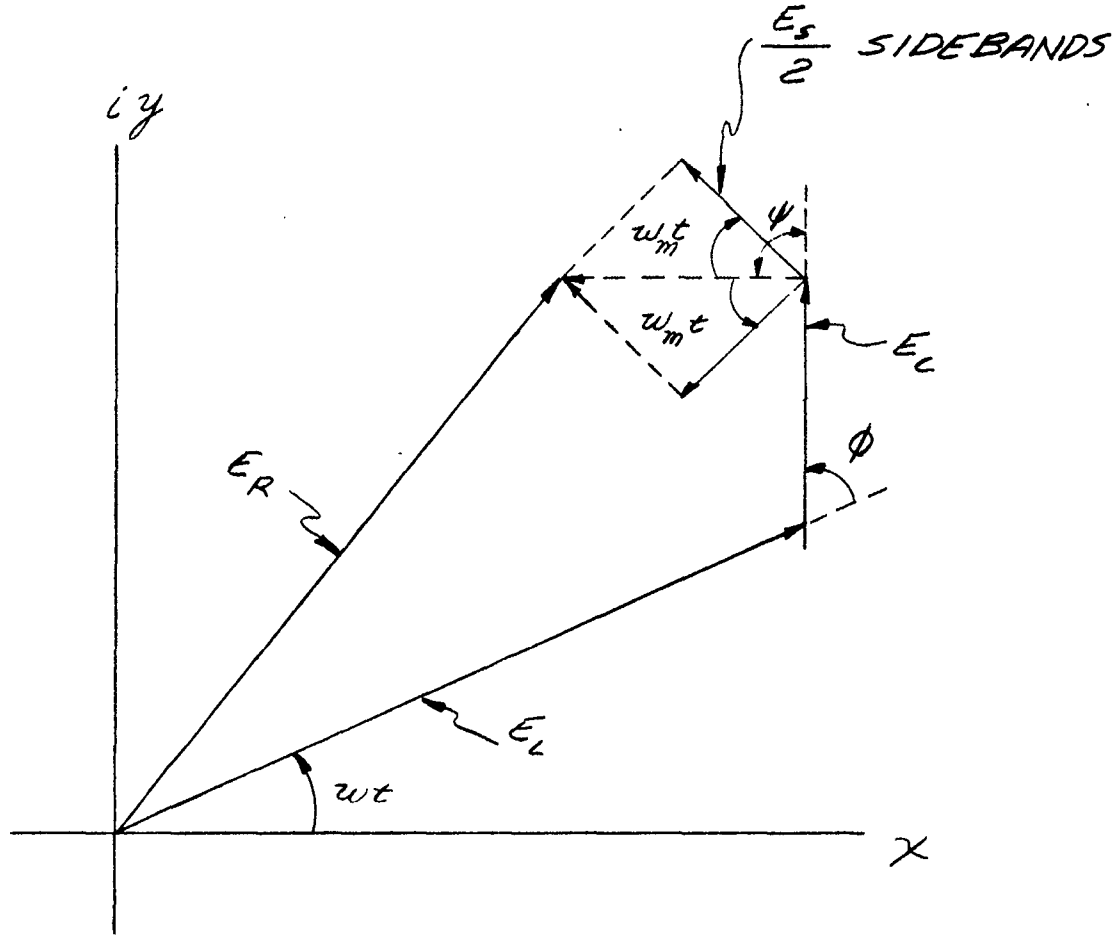

FIG. 2.4-7

HOMODYNE DETECTION WITH ARBITRARY PHASE ANGLE, ϕ.
RESULTANT FIELD OF MODULATED CARRIER AND LOCAL OSCILLATOR

The current flow

$$i \propto \overline{\mathcal{E}_R^2} \quad ,$$

where the averaging time includes many optical cycles, but is small compared with the period of the modulation cycle. Namely,

$$\frac{1}{\omega_m} >> T_{av} >> \frac{1}{\omega} \quad . \tag{2.4.3-3}$$

If we consider $E_L >> E_c$ and perform the averaging process:

$$\overline{\mathcal{E}_R^2} = \frac{E_L^2}{2} + E_L E_c \cos \phi + \left(\frac{m}{2}\right) E_L E_c \left\{\cos\left[\omega_m t + (\psi - \phi)\right] + \cos\left[\omega_m t - (\psi - \phi)\right]\right\} \tag{2.4.3-4}$$

which reduces to

$$\overline{\mathcal{E}_R^2} = \frac{E_L^2}{2} + E_L E_c \cos \phi + m E_L E_c \cos (\psi - \phi) \cos \omega_m t. \tag{2.4.3-5}$$

The term containing the homodyne-amplified signal is multiplied by the factor, cos $(\psi - \phi)$. This quantity must be made equal to unity to achieve maximum amplification. Thus, regardless of the form of modulation, demodulation can be obtained by adjusting the phase angle ϕ so that $\psi - \phi = 0$.

It should be noted that if $\psi - \phi$ is $\pi/2$, the heterodyne signal term may become zero. In the next section we begin to examine the effect of various perturbations on optical heterodyne signal.

2.4.3.2 Phase Stabilization Considerations

One of the basic difficulties in homodyning is the fluctuations that occur in the radiation phase of local oscillator and carrier. However, drift of the relative phase of the local oscillator with respect to the carrier, and the accompanying degradation of the homodyned signal, can be overcome in one of three ways:

A. The phase of the local oscillator can be adjusted electronically to yield a constant relative phase.

B. The transmission can be made single-sideband, reducing the effects of phase fluctuation.

C. Double detection of phase- and amplitude-modulation can be used to give an output independent of optical phase.

A. Electronic Control of Local Oscillator Phase. The relative phase of the local oscillator and incoming carrier can be servo-locked at either 0° or $\pi/2$ in the following way: A phase dither signal may be applied to the local oscillator by mechanical motion of the local oscillator reflector in one arm of the interferometer. This may be accomplished by mounting the mirror on a piezo-electric crystal and applying a small modulating voltage.

The beat frequency, on the square-law detector, between the local oscillator and the incoming carrier beams will contain only even harmonics of the dither frequency if the carrier and local oscillator are locked with 0° or π relative phase. Any deviation from 0° lock will cause the appearance of odd harmonics

whose signs will determine the direction of deviation, and whose amplitudes will be proportional to the magnitude of the phase deviation. With the relative phase of carrier and local oscillator at $\pm \pi/2$, only odd harmonics are present, and, similarly, deviation from phase quadrature gives rise to an error signal with the appearance of even harmonics of the dither frequency. In practice, only the fundamental or second harmonic need be monitored.

These effects can be seen analytically as follows:

The resultant field at the detector is

$$\mathcal{E}_R^2 = E_L^2 + E_c^2 - 2E_L E_c \cos\left(\frac{\pi}{2} - \phi\right). \qquad (2.4.3\text{-}6)$$

The dither on the local oscillator can be represented by replacing ϕ with

$$\phi = \phi_o + \delta \sin \omega_d t \qquad (2.4.3\text{-}7)$$

Thus

$$\mathcal{E}_R^2 = E_L^2 + E_c^2 - 2E_L E_c \cos\left(\frac{\pi}{2} - \phi_o - \delta \sin \omega_d t\right) \qquad (2.4.3\text{-}8)$$

$$\mathcal{E}_R^2 = E_L^2 + E_c^2 - 2E_L E_c \sin\left(\phi_o + \delta \sin \omega_d t\right) \qquad (2.4.3\text{-}9)$$

$$\mathcal{E}_R^2 = E_L^2 + E_c^2 - 2E_L E_c \sin \phi_o \cos\left(\delta \sin \omega_d t\right)$$

$$- 2E_L^2 E_c \cos \phi_o \sin\left(\delta \sin \omega_d t\right) \qquad (2.4.3\text{-}10)$$

For small deviations,

$$\phi_o \ll 1, \qquad \sin \phi_o \approx \phi_o, \qquad \cos \phi_o \approx 1 \ . \tag{2.4.3-11}$$

$$\mathcal{E}_r^2 = E_L^2 + E_c^2 - 2E_L E_c \, \phi_o \cos (\delta \sin \omega_d t) - 2E_L E_c \sin (\delta \sin \omega_d t) \tag{2.4.3-12}$$

since,

$$\cos (\delta \sin \omega_d t) \equiv J_o(\delta) + 2 \sum_{n=1}^{\infty} J_{2n}(\delta) \cos 2n \, \omega_d t \tag{2.4.3-13}$$

and

$$\sin (\delta \sin \omega_d t) = 2 \sum_{n=0}^{\infty} J_{2n+1}(\delta) \sin (2n+1) \, \omega_d t \ , \tag{2.4.3-14}$$

the homodyne current, which is proportional to $\mathcal{E}_r^2$, will have a component at the frequency $2\omega_d$ with its amplitude,

$$i_{\substack{\text{quadrature} \\ 2\omega_d}} \propto 4E_L E_c \, \phi_o J_2(\delta) \cos 2\omega_d t \ . \tag{2.4.3-15}$$

Thus, an error signal is developed at the output of the square-law detector which occurs at the frequency $2\omega_d$ and can be used to correct the phase difference and maintain quadrature between local oscillator and carrier.

A similar derivation shows that the fundamental, ω_d, can be used in the same manner to maintain lock at 0° or π. Fig. 2.4-8 is a block diagram of a possible circuit that could be used to maintain constant phase.

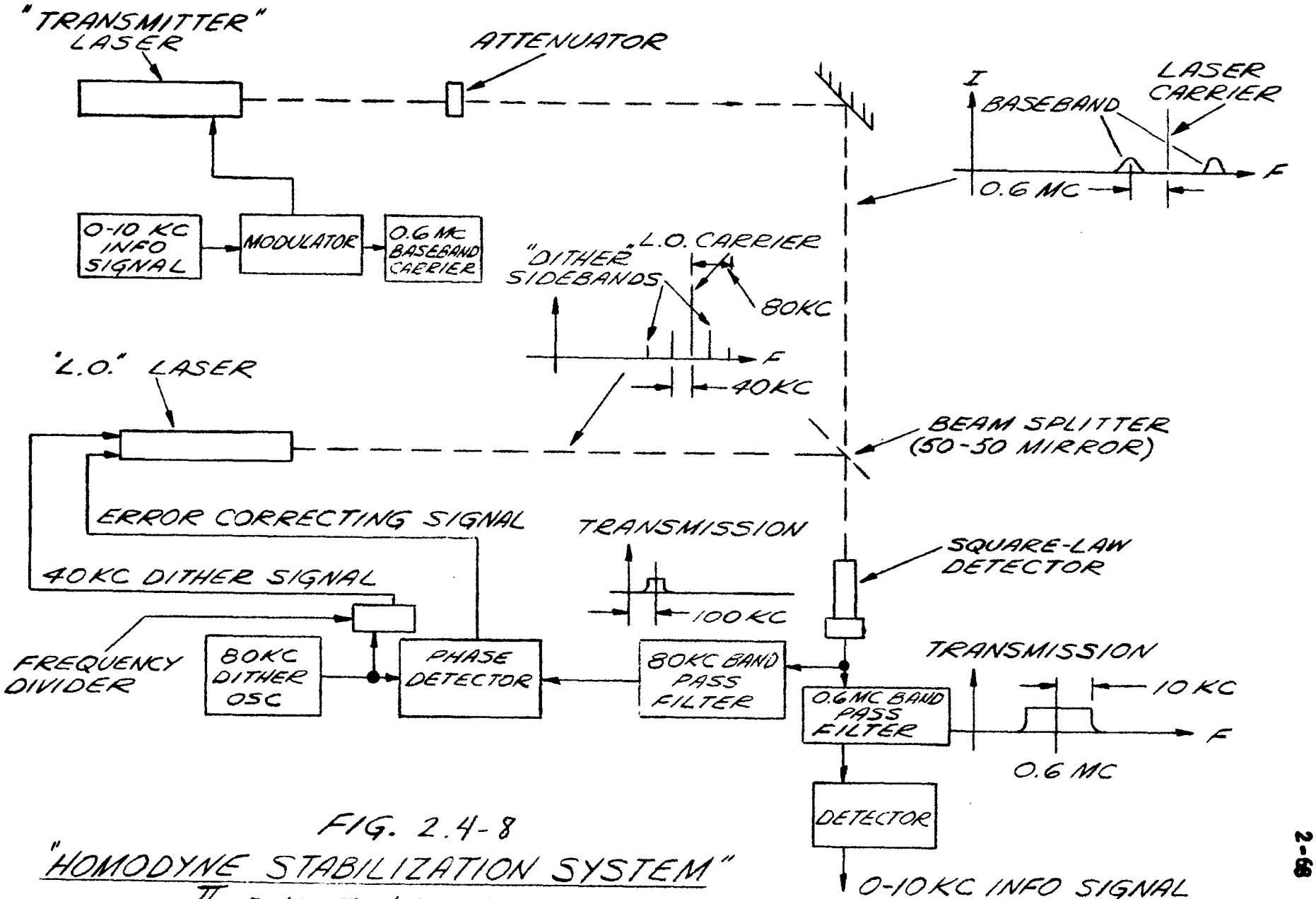

FIG. 2.4-8

"HOMODYNE STABILIZATION SYSTEM"

$\frac{\Pi}{2}$ PHASE LOCK

B. Single-Sideband Transmission Systems. The effect of phase fluctuations on homodyne amplification can be considerably reduced by the removal of the carrier and one sideband or one sideband alone. Eq. (2.4.3-2) gives the general expression for the resultant field at the detector. When one sideband is removed (single sideband unsuppressed carrier) this becomes

$$\mathcal{E}_r = \mathrm{Re}\left\{E_L e^{i(\omega t + \phi)} + E_c e^{i\omega t} + mE_c e^{i\left[(\omega+\omega_m)t + \psi\right]}\right\} \quad (2.4.3\text{-}16)$$

The detector current is than

$$i \propto \overline{\mathcal{E}_r^2} = \frac{E_L^2}{2} + E_L E_c \cos\phi + mE_L E_c \cos\left[\omega_m t + (\psi - \phi)\right] \quad (2.4.3\text{-}17)$$

In this case the homodyne amplitude is independent of phase. One difficulty with single sideband, unsuppressed carrier transmission is that fluctuations of phase angle ϕ will cause a change in the DC term, $E_L E_c \cos\phi$, and will contribute large noise signals at the fluctuation frequency.

When single sideband, suppressed carrier transmission is used, the resultant field is reduced to

$$\mathcal{E}_r = \mathrm{Re}\left\{E_L e^{i(\omega t + \phi)} + mE_c e^{i\left[(\omega+\omega_m)t + \psi\right]}\right\} \quad (2.4.3\text{-}18)$$

and the current is then

$$i \propto \overline{\mathcal{E}_r^2} = \frac{E_L^2}{2} + mE_L E_c \cos\left[\omega_m t + (\psi - \phi)\right] \quad (2.4.3\text{-}19)$$

As in the former case, (Eq. (2.4.3-17)), no phase-dependent amplitude variations occur in the homodyne signal. Moreover, the DC term, $E_L E_c \cos \phi$, and its associated phase-dependent noise no longer exist.

Another favorable point with regard to both forms of single sideband transmission is this: Over long paths through a dispersive medium the relative phase of the sidebands may become significantly shifted, resulting in a mixture of modulation, and a loss in information if the detector is phase-locked so as to accept only one form of modulation. With one sideband removed, this effect does not occur. Experimental arrangements for production of both the above forms of modulation are described in Sections 2.2.2-3 and 2.2.2-4.

Finally, the use of either type of single sideband transmissions results in a factor two reduction in the bandwidth necessary for transmission. This bandwidth conservation may, however, be of small consequence at optical frequencies.

C. Double Detection. Effects of phase fluctuations of signal beam relative to local oscillator beam can be completely removed by an optical compensation technique utilizing an arrangement with two detectors, each producing beats whose phase depends sinusoidally upon the relative phase angle, $\psi - \phi$. With an optical arrangement such that one detector produces a signal current

$$i_1^2 = K \cos^2 (\psi - \phi)$$

while the second detector produces a signal current

$$i_2^2 = K \sin^2 (\psi - \phi)$$

then the sum of these squared currents will be entirely independent of phase fluctuation.

An example of such an arrangement is shown in Fig. 2.4-9, where a relative phase difference of $\pi/2$ radians is introduced between the two halves of the local oscillator beam. Such a phase shift will result if one inserts into half of the beam a dielectric film with index of refraction, n, and thickness, t, such that

$$(n - 1)(t/\cos \theta) = \lambda/4$$

where the beam passes through the film at an angle, θ, with respect to the normal to the film. A precise $\pi/2$ phase difference can be obtained by adjusting the projected optical path difference by varying the orientation angle as shown. Note that when this double detection scheme is combined with the homodyne transceiver shown in Fig. 2.4-6, one must decrease the retardation film thickness by a factor of two in order to obtain the same $\pi/2$ phase difference.

If, now, after the addition of the signal beam each half is detected by a separate square-law detector, the resultant fields will be:

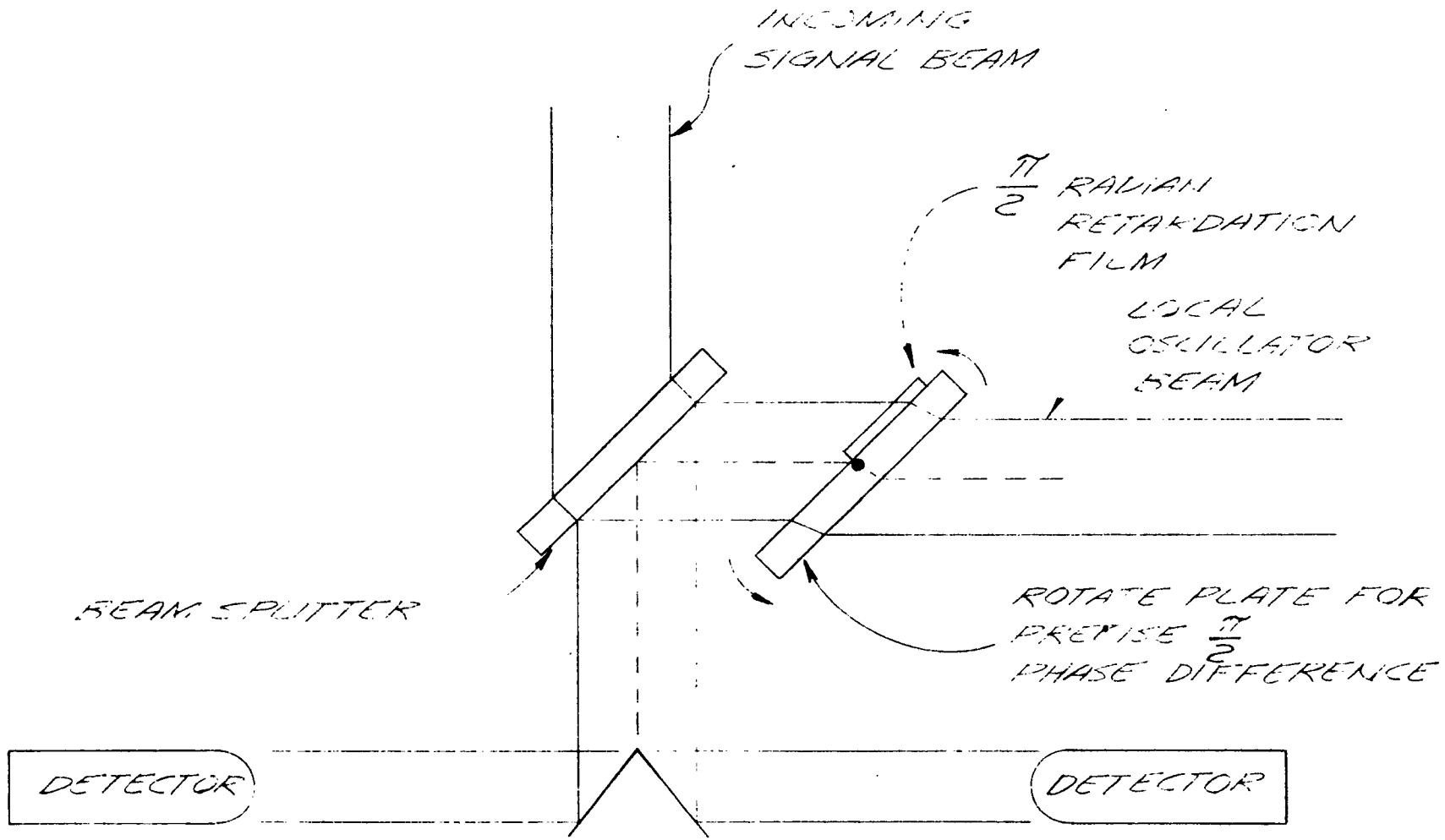

FIG. 2.4-9
OPTICAL ARRANGEMENT FOR
HOMODYNE DOUBLE DETECTION

$$\mathcal{E}_{r_1} = \mathrm{Re}\left\{E_L e^{i(\omega t + \phi)} + E_c e^{i\omega t} + E_c\left(\frac{m}{2}\right) e^{i\left[(\omega - \omega_m)t + \psi\right]} + E_c\left(\frac{m}{2}\right) e^{i\left[(\omega + \omega_m)t + \psi\right]}\right\} \tag{2.4.3-20}$$

$$\mathcal{E}_{r_2} = \mathrm{Re}\left\{E_L e^{i\left(\omega t + \phi + \frac{\pi}{2}\right)} + \ldots\ldots\ldots\ldots\ldots\ldots\ldots\right\} \tag{2.4.3-21}$$

The output currents will be

$$i_1 \propto \left[\frac{E_L^2}{2} + E_L E_c \cos\phi + mE_L E_c \cos(\psi - \phi) \cos\omega_m t\right] \tag{2.4.3-22}$$

$$i_2 \propto \left[\frac{E_L^2}{2} + E_L E_c \sin\phi + mE_L E_c \sin(\omega - \phi) \cos\omega_m t\right] \tag{2.4.3-23}$$

If each output is filtered of the low frequency terms, passed through a second square-law detector and then combined with the other output, the resulting current is

$$i_1^2 + i_2^2 = m^2 E_L^2 E_c^2 \cos^2\omega_m t \left[\cos^2(\psi - \phi) + \sin^2(\psi - \phi)\right] =$$

$$= m^2 E_L^2 E_c^2 \cos^2\omega_m t \tag{2.4.3-24}$$

As mentioned in Section 2.4.3, if a sub-carrier had been used to carry the information,

$$m = m_o(1 + k\cos\omega_k t) \tag{2.4.3-25}$$

where $\omega_k << \omega_m$. The summed currents give us a term

$$m_o^2 2E_L^2 E_c^2 \, k \cos \omega_k t \cos^2 \omega_m t \, . \qquad (2.4.3\text{-}26)$$

If we again average, such that

$$\frac{1}{\omega_k} > T_{av} > \frac{1}{\omega_m} \, , \qquad (2.4.3\text{-}27)$$

the output current has the term

$$m_o^2 E_L^2 E_c^2 \, k \cos \omega_k t \qquad (2.4.3\text{-}28)$$

without any phase terms that are related to the interferometer.

While this technique assures the absence of phase fluctuations, the losses encountered in splitting the beam, in double modulation and detection, and in the differences between detectors may be prohibitive.

2.4.3.3 Coherence in Optical Heterodyne Detection

The basic function of the interferometer is to provide a means of achieving spatial coherence between the signal and local oscillator beams across the surface of the optical square-law detector. A radio frequencies the detectors used are small compared to the wavelength of the radiation and so the phase errors, due to imperfect spatial coherence, have negligible effect. The equation for the heterodyne current, taking into account spatial factors, may be written as

$$i_{ac} = \frac{2i_{dc}}{A} \int \frac{\vec{E}_{lo} \cdot \vec{E}_s}{E_{lo}^2} \cos \left[(\omega_{lo} - \omega_s)t + (\phi_{lo} - \phi_s)\right] ds \qquad (2.4.3\text{-}29)$$

where ($\rightarrow$) signifies the complex polarization and the ϕ_{lo}, ϕ_s are phase angles which are a function of position only.

When perfect spatial coherence is obtained, Equation 2.4.3-29 reduces to the more familiar form:

$$i_{ac} = 2i_{dc} \frac{E_s}{E_{lo}} \cos \left[(\omega_{lo} - \omega_s)t + \phi\right] \qquad (2.4.3\text{-}30)$$

Temporal coherence of signal and local oscillator beams is automatic in the homodyne system, provided the interferometer arm spacing does not exceed the coherence length of the oscillator.

The coherence length is related to the LASER linewidth, $\Delta\nu$, through the expression

$$L_{coherence} = \frac{c}{2\pi\Delta\nu} \qquad (2.4.3\text{-}31)$$

The theoretical value of $\Delta\nu$ is given by the Townes formula:

$$\Delta\nu_{osc} = \frac{2\pi h\nu}{P} (\Delta\nu_c)^2 \sim 0.01 \text{ cycles/sec} \qquad (2.4.3\text{-}32)$$

We have measured an upper limit to the value of $\Delta\nu$ by measuring the

self-beats in the LASER noise frequency spectrum. No self-beats were observed at frequencies down to 5 cps, indicating that the linewidth of our He-Ne LASER is less than 10 cps and the coherence length is at least 5×10^6 meters. For single-mode operation, temporal effects can be neglected for separations that are small compared to the coherence length. However, in multimode operation temporal coherence becomes a limiting factor, for one cannot simultaneously satisfy the in-phase requirements between local oscillator and carrier with several modes present. The effective coherence length is determined by

$$\frac{c}{2\pi\Delta\nu_{mm}}$$

where $\Delta\nu_{mm}$ is the frequency spread between the most widely separated modes, rather than the mode width itself. Since the separation can approach 1 kMc, coherence lengths can become effectively as small as several centimeters in multimode operation.

We have qualitatively observed a degradation of the heterodyne amplification with the appearance of more than one mode, and our result, which showed that amplification was $P_L P_S$, where P_L = power of the local oscillator, P_S = power of signal beam, was verified specifically for single-mode operation. (See Sect. 2.4.3.5).

Spatial incoherence between the local oscillator and signal beam can occur in many ways, namely:

A. Improper angular alignment of the interferometer.

B. Mixture of polarizations.

C. Displacement of the beams on the photocathode.

D. Different shapes of the signal and local oscillator wavefronts.

A. Improper Angular Alignment. If the signal and local oscillator beams are not parallel, they cannot be focussed down to completely overlapping Fraunhofer diffraction spots, and hence the heterodyne beat signal is reduced by the ratio of overlapping area to the area of the Fraunhofer spot.

It should be noted that focussing in itself does not affect the heterodyne signal. For example, if the two beams are allowed to fall unfocussed on the square-law detector, the reduction of signal occurs as well because the relative phase changes as a function of position on the detector. This loss is equivalent to the focussed case. In Appendix B is an analysis of the quantitative variations of heterodyne signal, as a function of tip angle between the beams, under the following conditions:

1. The phase fronts of both local oscillator and signal beam are plane and constant.
2. The plane of polarization of both beams is the same,
$$\vec{E}_S \cdot \vec{E}_L = \left|\vec{E}_S\right| \cdot \left|\vec{E}_L\right| .$$
3. The phase difference $(\phi_L - \phi_S) = \phi(x)$ varies linearly across the aperture.

4. The two beams have the same angular frequency, $\omega_L = \omega_s$.
5. The beams have equal overlapping circular cross sections, $R_s = R_{lo} = r$.
6. The relative phase of the two beams is adjusted to give maximum signal output.

These conditions are approximately fulfilled for the LASER that is employed in our experiments.

Fig. 2.4-10 shows the result of the analysis: i.e., the degradation (or normalized amplification) vs. wavefront tip angle. The reduction of spatial coherence due to angular misalignment can be minimized by the introduction of retroreflecting mirrors in the interferometer. Cube corners, used for both signal and local oscillator mirrors automatically insure angular alignment of the two beams, but introduce difficulties in polarization: One property of a cube corner is that, when plane polarized light is incident upon it, the reflected wave is generally elliptically polarized. The axes of the ellipse are determined by the angle made by the polarization with the respective cube axes, and the particular sextant on which the wave is incident. Thus, in order to maintain spatial coherence with respect to polarization, it is necessary to orient the cube axes such that polarization changes at the local oscillator mirror are equivalent to the change incurred at the signal mirror. This amounts to aligning the cubes with respect to rotation about the interferometer optic axis.

Therefore, rather than having a possible two dimensions of tilt to contend with, as in the case of plane mirrors, there is

FIG. 2.4-10

HETERODYNE AMPLIFCATION, γ VS ANGULAR MISALIGNMENT ANGLE, θ

$$\theta = \frac{\lambda}{2\pi r}\,\Delta$$

$$\gamma = J_0(\Delta) + J_2(\Delta)$$

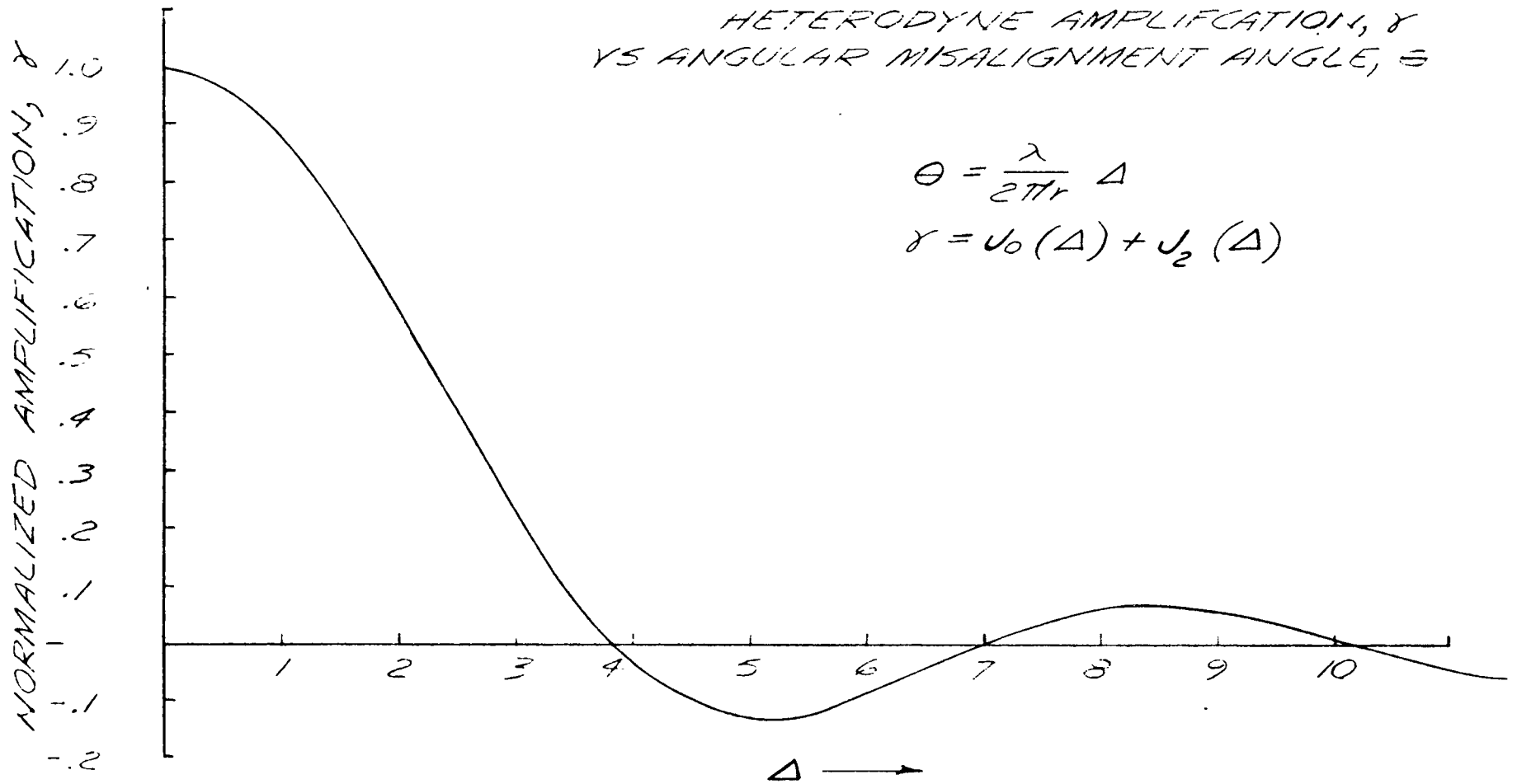

only a single adjustment necessary with cubes. It should be noted that the tolerance on the alignment of the cube rotation is of the order of degrees, whereas tilt of plane mirrors must be adjusted within fractions of a minute. We have constructed a Twyman-Green interferometer with cube corner mirrors and are in the process of evaluating its increased alignment stability.

B. Mixture of Polarization. If the signal beam passes through an optically active medium, or reflects from a retroreflector having either a dielectric or metallic surface, in general a change in the state of polarization occurs. Since heterodyne beats can only arise from like polarizations, any change of polarization state of the signal beam relative to the local oscillator results in a loss of heterodyne signal. The appearance of energy in a different polarization is equivalent to the appearance of new spatial modes. Thus, as mentioned earlier, when retroreflectors are incorporated in the heterodyne system, they must be adjusted to polarize the beams in a like manner.

C. Displacement of the Beams on the Photocathode. This effect can occur with parallel beams when the beams are not focussed to a Fraunhofer spot. If the signal beam is parallel to the local oscillator beam, but not coaxial to it, as may occur when displaced upon reflection from a retroreflector, the two beams may not completely overlap, producing a loss in signal. This effect is partially removed by focussing the beams to a Fraunhofer spot, since

the focussing is equivalent to allowing the beams to diffract over long distances where they will coalesce and interfere. The introduction of a Fraunhofer pinhole in a screen placed at the focus of the lens with the detector behind it has a further advantageous effect: Since only light parallel to the local oscillator beam will pass through the pinhole, background radiation incident on the detector will be limited to that portion which is spatially coherent with the local oscillator beam. Thus, beside partially rectifying spatial incoherence between signal and local oscillator, focussing to a Fraunhofer spot allows the selective spatial filtering of background radiation.

D. Different Shapes of Local Oscillator and Signal Wavefronts. If two waves are spatially coherent at any given surface, they will be coherent for all surfaces throughout space, their relative phase being constant. Thus relative variations in the shape of the phase fronts constitutes a form of spatial incoherence and is similar in many respects to angular misalignment since, in both cases, the effect on the heterodyne signal is the generation of photocurrents of varying phases from different parts of the detector surface.

This effect occurs, for example, when one uses a spherical LASER resonator in a transceiver homodyne system with unequal arms. Here the local oscillator wavefront is approximately a spherical wavefront, because of its proximity to the LASER cavity, while the signal, which has traversed a large distance, can be appropriately represented as a plane wave. This particular error can be overcome

by placing a convergent lens of proper focal length in the local oscillator arm. The addition of the lens corrects the local oscillator wavefront, bringing it into coherence with the signal beam wavefront.

When one wave becomes distorted in a random manner with respect to the other, for example by thermal air turbulence, the heterodyne signal will be degraded in an irreparable way. Effects of air turbulence were observed in a qualitative manner with the laboratory interferometer apparatus. It was found that the heterodyne signal varied from maximum to minimum at a frequency of about 1 cycle/sec. However, part of these variations were due to longitudinal fluctuations of phase which can be corrected by techniques that are described in Section 2.4.3.2. Transverse fluctuations, however, cannot be corrected and it will be necessary to make field measurements with a system that is unaffected by longitudinal fluctuations to determine the magnitude of the degradation of coherence when a signal is passed through the atmosphere.

Another factor that is related to spatial coherence is the effect of vibrations on the heterodyne detector. The present laboratory system is built on a base consisting of 4 tons of bricks, spaced by thick insulating material which, in turn, is covered by a 2-ton granite slab. This large mass is floated on airplane inner tubes to give maximum shock insulation. It is observed, however, that vibrations of the interferometer elements, acoustically induced, modulate the heterodyne signal by changing the relative phases of

the two beams. This indicates that extremely critical mechanical design will be required for any field instrument.

2.4.3.4 Experimental Verification of Homodyne Demodulation

Experimentally, we have observed the demodulation of a phase modulated signal in a homodyne system consisting of a LASER beam split into two beams and recombined as shown in Fig. 2.4-6. This interferometer arrangement makes possible the physical separation of the LASER output into a "carrier" and "local oscillator" beam which are automatically frequency-stabilized with respect to each other. Phase modulation is impressed on the signal beam by modulating the mirror position by means of a piezo-electric element. This mechanical modulator can produce phase modulation up to 500 kc/sec. The relative phase of the carrier and local oscillator is grossly adjustable by means of an extremely fine Fabry-Perot adjustment screw on one mirror, which gives controllable motions to $\lambda/50$, or a phase adjustment of 7°. The demodulated signal could not be observed if the local oscillator beam was blocked, since the square-law detector cannot demodulate phase modulation without the homodyne action of the local oscillator.

The depth of modulation that can be used in this system is limited by the requirement for linearity. The homodyned current, which can be written as (see Eq. (2.4.3-7)):

$$i \propto E_L E_c \sin (\delta \sin \omega_m t) \qquad (2.4.3\text{-}32)$$

when carrier and local oscillator are in phase quadrature, will only be a linear representation of the modulation, in, the region where $\delta << 1$. The expansion for an arbitrary depth of modulation, δ, gives

$$i \propto E_L E_c \sum_{n=0}^{\infty} J_{2n+1}(\epsilon) \sin (2n+1)\omega_m t \qquad (2.4.3\text{-}33)$$

As the value of $\delta \to 1$ the percentage of harmonic distortion increases, with a larger portion of the information energy found in the odd harmonics. These facts were verified experimentally by examining the homodyned output with a spectrum analyzer, and measuring the percentage of the various odd harmonics as a function of δ. The measured percent modulation was in good agreement with with estimates made from oscilloscope traces. Theoretical considerations also indicate that when the relative phase of carier and local oscillator is changed to either 0 or $\pi°$, only even harmonics of the signal should be present. This, too, was verified. It should be mentioned that, although several schemes for demodulating phase-modulated light have been proposed, this is the first time, to our knowledge, that phase- or frequency-modulated light has been detected experimentally.*

---

*P. Rabinowitz, S. Jacobs, R. Targ, G. Gould, Proc. IRE 50, 3265, (1962).

2.4.3.5 Experimental Verification of Heterodyne Amplification

The principle of heterodyne amplification was verified with the arrangement shown in Fig. 2.4-6, including several calibrated intensity attenuators with which to vary the signal beam power. The heterodyne signal current was measured for a wide range of signal beam powers, keeping the local oscillator beam power constant. We have verified experimentally that, for single-mode operation,

$$i_{beat} \propto \sqrt{P_L P_S}$$

where P_L = local oscillator power,

P_S = signal beam power.

2.4.3.6 Experimental Verification of Theoretical Heterodyne S/N

At the time of writing, preliminary data has just been taken which compares the experimental S/N with the theoretical value (see Eq. 1.3-8):

$$(S/N)_{\text{power ratio}} = \frac{\eta P_s}{h\nu\ \Delta f}$$

where P_s is the single-sideband (signal) power and $P_s \ll P_L$ is assumed. For the more general case, Eq. (1.3-4) leads to

$$(S/N)_{\text{power ratio}} = \frac{P_L P_S}{P_L + P_S} \frac{\eta}{h\nu\ \Delta f} \qquad (2.4.3\text{-}34)$$

or

$$\boxed{(S/N)_{\text{voltage ratio}} = \left(\frac{P_L P_S}{P_L + P_S} \frac{\eta}{h\nu\ \Delta f} \right)^{1/2}} \qquad (2.4.3\text{-}35)$$

For phase-modulation, through an angle $\pm\ \phi$ radians, the relative amplitude of the first sidebands ($n = \pm\ 1$) is proportional to the Bessel function, $J_1(\phi)$. When these two sidebands are mixed with the fundamental (local oscillator), both contribute to the amplitude of the beat frequency term (called $[\omega_{LO} - \omega_S]$ in Eq. 1.3-3). Thus, for phase-modulation with double sidebands, the single-sideband analysis of Section 1.3 may be used, provided the signal power is modified as follows:

$$E_S \rightarrow 2J_1(\phi)\ E_{S_o}\ , \qquad (2.4.3\text{-}36)$$

where E_{S_o} is the amplitude of the unmodulated signal beam (see Eq. 1.301), and

$$P_S \rightarrow \left[2J_1(\phi)\right]^2 P_{S_o} \qquad (2.4.3\text{-}37)$$

where P_{S_o} is the power of the unmodulated signal beam (see Eq. 1.3-1).

For the case where $P_L \gg P_S$, the final expression becomes:

$$\boxed{(S/N)_{voltage} = 2J_1(\phi)\left(\frac{\eta P_{S_o}}{h\nu\ \Delta f}\right)^{1/2}} \qquad (2.4.3\text{-}38)$$

The experimental arrangement used to verify the above relationship is shown in Fig. 2.4-11. The 1.15μ He-Ne LASER was adjusted to provide a single-mode output beam whose power level was 6μw. The signal beam was phase-modulated, at 1000 cps, by means of a piezo-electrically driven mirror. The modulation depth, ϕ, was approximately 0.6 radians, as estimated from the C.R.O. screen. The spectrum analyzer used was a Marconi (Model TF455D/1) with Δf = 4 cps).

RCA 7102 photomultiplier #3 (see Table 2.4-2) was used, at 1100 volts, its face masked to 3/8" in the center of the photo-sensitive surface. The responsivity of this masked phototube, including an optical narrow-band filter, centered at λ = 1.15μ, is

$$R_{\text{phototube } \#3} = 0.27 \text{ amp/watt.}$$

The quantum efficiency of tube #3 is

$$\eta = 2.3 \times 10^{-5} \text{ electrons/photon.}$$

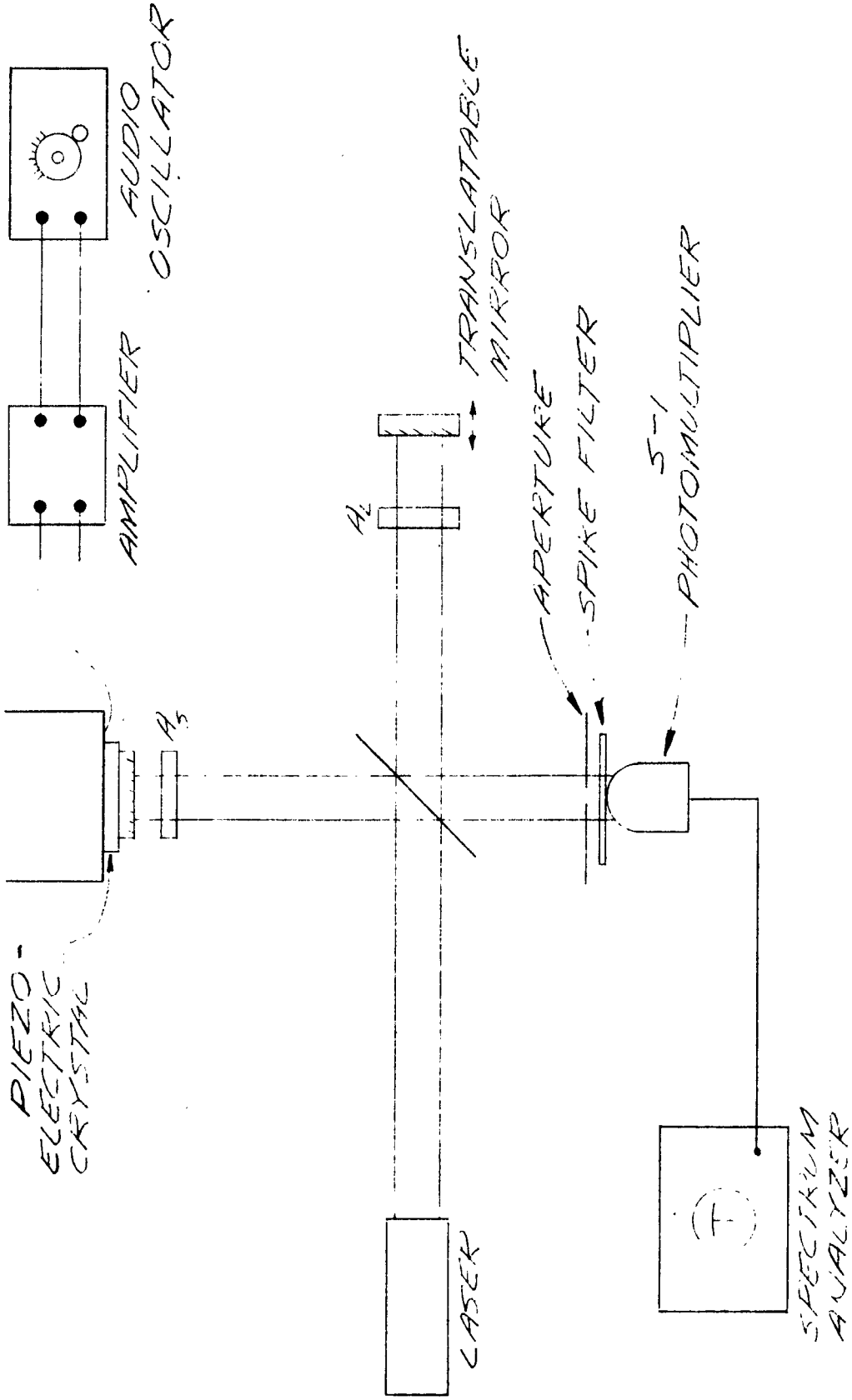

FIG. 2.4-11

ARRANGEMENT FOR MEASURING S/N VS. R.C.

Plane-parallel, calibrated attenuators were placed in the signal beam to vary the signal beam power.

Table 2.4-4 lists the beam powers incident on the detector sensitive surface, the optical power attenuations used to vary the signal beam power and the measured signal and noise values. Fig. 2.4-12 shows the measured vs. theoretical S/N voltages.

We would like to re-emphasize the fact that these data are preliminary. Time does not allow the inclusion in this report of measurements extended to a wider range of power levels. Further measurements are being made, to include more numerous points with reduced uncertainty.

Nevertheless, these data show agreement with theory within less than a factor of 2, which is probably within the present experimental error.

An additional experiment, performed with the same apparatus, demonstrates the preservation of S/N for fixed signal beam power and varying local oscillator power. The data, listed in Table 2.4-5 and plotted in Fig. 2.4-13 show clearly the constancy of S/N, provided $i_{LO} >> i_{background}$.

TABLE 2.4-4

Summary of Quadrature S/N Measurements

P_L (μw)	Signal Power Attenuation	P_S (μw)	S (mv)	N (mv)	$(S/N)_{meas}$	$(S/N)_{theor} = \left(\frac{2J_1(\phi)^2 P_S P_L}{P_L + 2J_1(\phi)^2 P_S} \frac{\eta}{h\nu\Delta f} \right)^{1/2}$
1.0	x 1.000	0.70	116	.12	970	1880
1.0	x .026	.018	40	.075	530	410
1.0	x .0064	.0044	11	.075	147	220
1.0	x .0024	.0017	7.5	.075	100	128

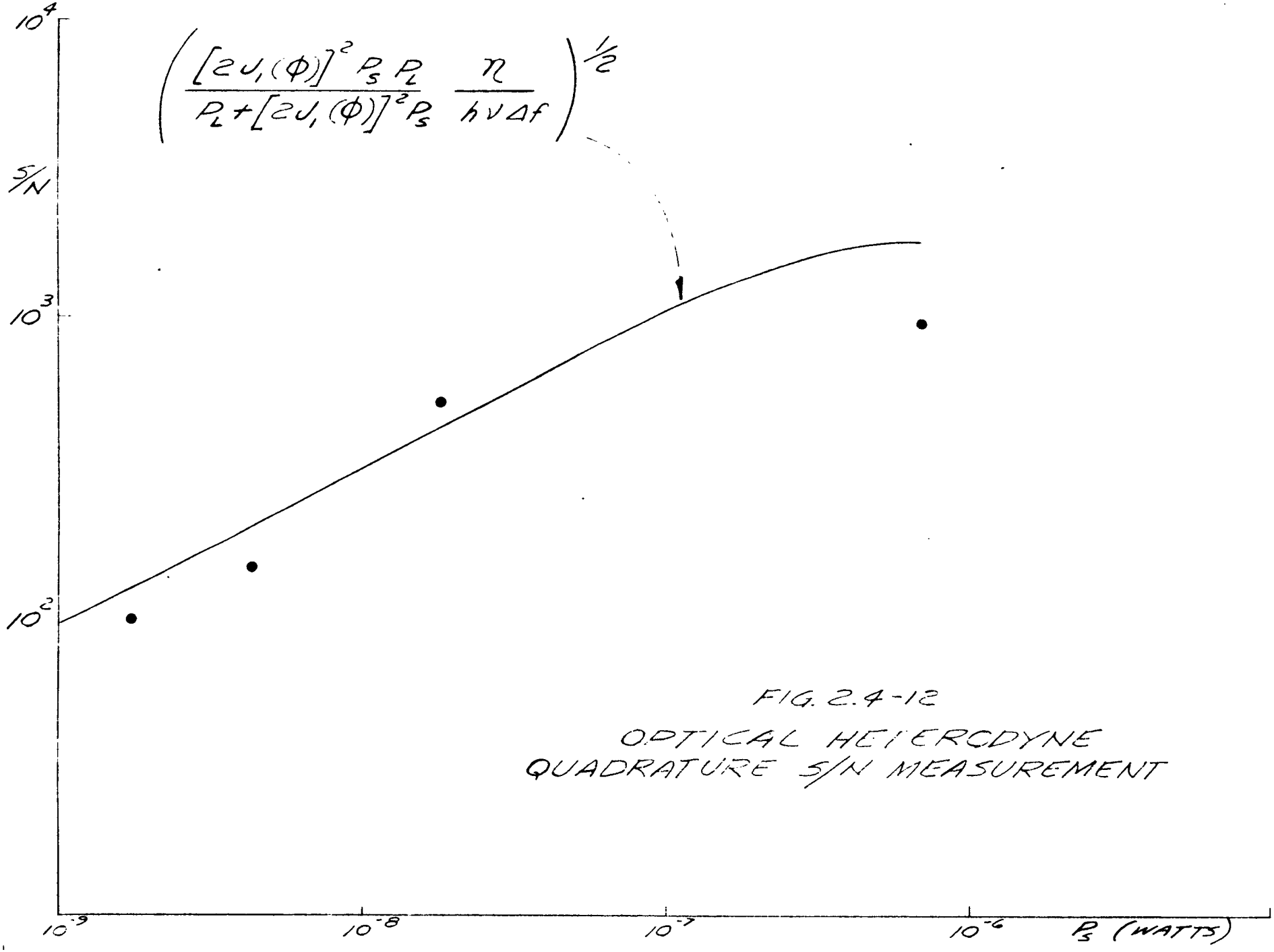

FIG. 2.4-12

OPTICAL HETERODYNE
QUADRATURE S/N MEASUREMENT

TABLE 2.4-5

Signal-to-noise ratios with attenuation

Initial Power		Attenuation		Power at Detector		Signal and Noise		S/N
P_{L_o}	P_{S_o}	A_L	A_s	$P_L = P_{L_o}/A_L$	$P_s = P_{S_c}/A_s$	S	N	S/N
1.4μw	1.3μw	1	700	1.4μw	.0019μw	30 mv	.6 mv	180
1.4	1.3	1.83	700	.77	.0019	21	.11	180
1.4	1.3	5.74	700	.24	.0019	7	.04	175
1.4	1.3	34.4	700	.04	.0019	4	.03	133
1.4	1.3	77.5	700	.018	.0019	3	.035	86
1.4	1.3	310	700	.0045	.0019	1.2	.03	40

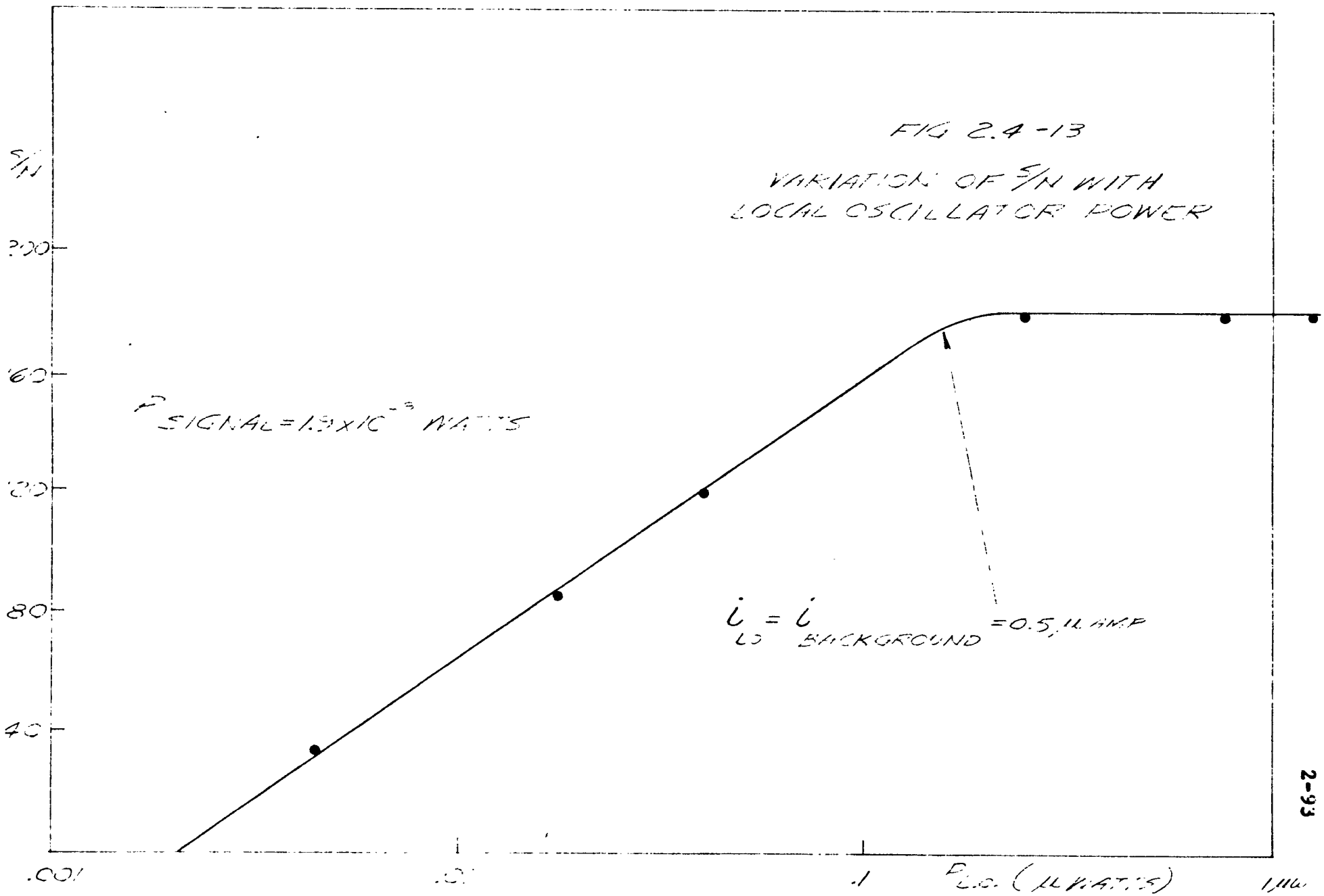
FIG 2.4-13
VARIATION OF S/N WITH
LOCAL OSCILLATOR POWER
S/N
100
60
20
80
40
$P_{SIGNAL} = 1.9 \times 10^{-9}$ WATTS
$i_{LO} = i_{BACKGROUND} = 0.5$ MA AMP
.001
.01
.1
$P_{L.O.}$ (MILLIWATTS)
1 MW

3.0 Conclusions and Recommendations

The original program for study of optical heterodyning called for a discussion of the theory and experimental test of the optical heterodyne detection technique. Before these measurements could be carried out it was necessary to establish techniques for using a Twyman-Green interferometer with a single-mode LASER, to measure LASER modulation and detection characteristics, and to expand and refine the theory to cover FM, AM, etc.

As stated in Section 1-1, the following steps have now been completed:

1. The theory of heterodyning was refined and applied to single-sideband, AM, and FM detection; the expected signal-to-noise ratios were obtained.
2. The fluctuations in the photoemitted current generated by a LASER were measured between 10 cps and 10^8 cps. As predicted, the fluctuations did not exceed shot noise. This is essential if the signal-to-noise ratio is to be preserved in heterodyne detection.
3. LASER characteristics were investigated.
4. Photomultiplier characteristics were investigated.
5. Amplitude- and phase-modulated light beams were homodyne-detected.
6. Heterodyne amplification was measured and found to be in agreement with theory.

7. Theory was developed for production of single-sideband modulation (suppressed or unsuppressed carrier).
8. Theory was developed for double detection to eliminate differential optical path length fluctuations.
9. Electro-optic and electro-strictive light modulators were constructed.
10. Signal-to-noise measurements under a variety of conditions were initiated but not yet completed.

The remaining tasks include the completion of the signal-to-noise measurements. We will also investigate the use of cube corner reflectors for automatic adjustment of the returning beam direction. This will be necessary for the extension of the interferometer arm to great distances. Finally we will investigate the use of a pinhole to discriminate against background illumination and to correct spatial incoherence between local oscillator and signal.

So far, predictions have been satisfactorily confirmed. During the course of this work, it has become clear that long wavelength transmission has many advantages, including easier optical tolerances, (LASER, modulator, and antenna mirror) which lead to greater stability, great single-mode power obtainable, better ultimate S/N for given power, and optimum atmospheric transmission in the wavelength region near 4μ. With the advantages of heterodyne detection, it is possible to work in the near infra-red region with available detectors which have high quantum efficiency out to 7μ. However, high quality optical materials with high transmission become less plentiful at longer wavelengths.

We have learned, qualitatively, that atmospheric effects cause serious deterioration of the heterodyned S/N. In order to elucidate the practical limitations imposed by atmospheric and other effects we recommend setting up an experimental communications link. Technique has reached the point where this seems appropriate. The primary purpose envisaged for this experimental link would be to determine the optimum solution to the problem of dispersion. The three methods include:

1. Phase lock of local oscillator arm to signal sidebands--already accomplished under Contract AF33(657)-8060.
2. Double detection.
3. Single-sideband transmission.

One or more of these methods should be tried out, at a range of about 1 Kilometer, by extending the "signal beam" arm of the interferometer and utilizing cube corner retro-reflectors. Operation at low frequency (1 - 10 Mc) will be first attempted since it is the easiest and least costly means for facilitating the measurements of atmospheric phenomena. After first investigating the problems due to fluctuations, we will then simulate wideband dispersion and other effects.

In general, it is our feeling that optical heterodyning will prove to be most useful in extreme range systems where the weak incoming signal would otherwise be lost in incoherent background and detector noise. In such applications heterodyne detection will allow fullest use of the bandwidth which is limited by the

signal-to-noise-in-signal ratio to modest values. Convenient, relatively narrow-band modulators and detectors, which have been mentioned in this report, will be useful in these applications. Also, in such extreme range systems, the bulk of the transmission path will lie outside the turbulent atmosphere.

For shorter range, broadband systems, heterodyne detection may also prove to be the most convenient method of detection. An array of LASER local oscillator heterodyne detectors, each tuned to the frequency of an information channel, may be used to detect and separate channels in an extremely broadband system. Such a technique will make possible total information bandwidths which exceed the bandwidth of available photodetectors. The analogous scheme at the transmitter can similarly multiply the bandwidth of available modulators and the power of existing LASERs. Investigations of the merits of such a multiplixing scheme and other applications of heterodyne detection are being continued.

APPENDIX A

Details of the Single-Sideband Suppressed Carrier Optical Modulation Analysis

I. Propagation of a circularly polarized ray through a birefringent crystal.

With the notation defined in Section 2.2.2.3, the electric vector of an incoming circularly polarized ray, $\binom{\text{RHCP}}{\text{LHCP}}$, is (Eq. 2.2.2-1):

$$E_1(z,t) \equiv Ae^{\pm}(\omega t - kz) \tag{A-1}$$

We decompose this ray into perpendicular plane polarized components which are polarized along the principal axes of the crystal which are oriented at an angle $+\Omega$ with respect to the standard coordinates:

$$\begin{aligned} E_{1r}(z,t) &\equiv e^{-i\Omega}E_1(z,t) \\ &= e^{\pm i(\omega t - kz \mp \Omega)} \\ &= \cos(\omega t - kz \mp \Omega) \pm i \sin(\omega t - kz \mp \Omega). \end{aligned} \tag{A-2}$$

The two components propagate at different velocities, through the crystal of length ℓ, and the difference in optical path length, $(n_x\ell - n_y\ell)$ yields the phase retardation:

$$2\beta = 2\pi (n_x - n_y)\ell/\lambda \quad .$$

Thus, after traversing the crystal, the electric vector is:

$$E_{2r}(z,t) = A \cos(\alpha' - \beta) \pm i A \sin(\alpha' + \beta) \qquad \text{(A-3)}$$

where

$$\alpha' = \omega t = k(z - \ell) - \frac{2\pi\ell}{\lambda}\left(\frac{n_x + n_y}{2}\right) \mp \Omega \equiv \alpha \mp \Omega$$

The desired result is obtained by separating right and left circularly polarized components, and rotating back to the standard coordinate system. First, we expand,

$$E_{2r}(z,t) = \frac{A}{2}\left\{e^{i\alpha - i\beta} + e^{-i\alpha + i\beta} \pm e^{i\alpha + i\beta} \mp e^{-i\alpha - i\beta}\right\} \qquad \text{(A-4)}$$

Then recombine, using $\alpha' = \alpha \mp \Omega$,

$$E_{2r}(z,t) = Ae^{\pm i\alpha - i\Omega}\cos\beta + Ae^{\mp i(\alpha - \frac{\pi}{2}) + i\Omega}\sin\beta \qquad \text{(A-5)}$$

The rotation back to the standard coordinate yields:

$$E_2(z,t) = e^{i\Omega}E_{2r} = Ae^{\pm i\alpha}\cos\beta + Ae^{\mp i(\alpha - \frac{\pi}{2} \mp 2\Omega)}\sin\beta \qquad \text{(A-6)}$$

which is Eq. 2.2.2-2.

II. Details of "A pair of phased oscillating birefringent crystals".

The details of applying Eq. 2.2.2-2 twice as described in Section 2.2.2-3-C are tedious but straightforward. With a RHCP ray incident, the output of the first crystal, wherein $\Omega = 0$ and $\beta_1 = (\pi n_o^3 rV/\lambda) \sin \omega_m t \equiv (\beta_o \sqrt{1/2}) \sin \omega_m t$, is

$$A^{-1}E_2(z,t) = e^{i\alpha_1} \cos \beta_1 + e^{-i(\alpha_1 - \frac{\pi}{2})} \sin \beta_1 . \qquad \text{(A-6)}$$

The output of the second crystal is obtained by applying Eq. 2.2.2-2 with $\Omega = + \pi/4$ and $\beta_2 = (\beta_o/\sqrt{2}) \cos \omega_m t$, separately to the two terms of Eq. (A-6):

$$A^{-1}E_3(z,t) = e^{i\alpha_2} c_1 c_2 + e^{-i(\alpha_2 - \pi)} c_1 s_2 + e^{-i(\alpha_2 - \frac{\pi}{2})} s_1 c_2 + e^{i(\alpha_2 - \frac{\pi}{2})} s_1 s_2 \qquad \text{(A-7)}$$

where $c_1 = \cos \beta_1$, $s_2 = \sin \beta_2$, etc.

Collecting RHCP terms and LHCP terms, we obtain

$$A^{-1}E_3(z,t) = e^{i\alpha_2}(c_1 c_2 + e^{-i\frac{\pi}{2}} s_1 s_2) + e^{-i(\alpha_2 - \frac{\pi}{2})}(s_1 c_2 + e^{i\frac{\pi}{2}} s_2 c_1) . \qquad \text{(A-8)}$$

If one combines the identities:

$$\begin{Bmatrix} c_1 c_2 \\ s_1 s_2 \end{Bmatrix} = \frac{1}{2} \left[\cos(\beta_1 - \beta_2) \pm \cos(\beta_1 + \beta_2)\right] \qquad \text{(A-9)}$$

Rome Air Development Center, Griffiss AF Base, N.Y.
Rpt.No. RADC-TDR-62-491. HETERODYNE DETECTION IN OPTICAL COMMUNICATION. FIRST TECHNICAL NOTE.
30 Nov. 62, 141p., incl. illus., tables.

Unclassified Report

The properties of optical heterodyne detection are analyzed and measured using a LASER and a Twyman-Green interferometer. It is shown that heterodyne amplification preserves the signal-to-noise ratio in the detected difference frequency in

1. Optical Communication
2. Heterodyne detection
3. Lasers, Single mode

I. AFSC Project 4519 Task 451905
II. Contract AF30 (602)-2591
III. Technical Research Group Inc. Syosset, N.Y.
IV. J.Latourrette, S.Jacobs, G.Gould

Rome Air Development Center, Griffiss AF Base, N.Y.
Rpt.No. RADC-TDR-62-491. HETERODYNE DETECTION IN OPTICAL COMMUNICATION. FIRST TECHNICAL NOTE.
30 Nov. 62, 141p., incl. illus., tables.

Unclassified Report

The properties of optical heterodyne detection are analyzed and measured using a LASER and a Twyman-Green interferometer. It is shown that heterodyne amplification preserves the signal-to-noise ratio in the detected difference frequency in

1. Optical Communication
2. Heterodyne detection
3. Lasers, Single mode

I. AFSC Project 4519 Task 451905
II. Contract AF30 (602)-2591
III. Technical Research Group Inc. Syosset, N.Y.
IV. J.Latourrette, S.Jacobs, G.Gould

Rome Air Development Center, Griffiss AF Base, N.Y.
Rpt.No. RADC-TDR-62-491. HETERODYNE DETECTION IN OPTICAL COMMUNICATION. FIRST TECHNICAL NOTE.
30 Nov. 62, 141p., incl. illus., tables.

Unclassified Report

The properties of optical heterodyne detection are analyzed and measured using a LASER and a Twyman-Green interferometer. It is shown that heterodyne amplification preserves the signal-to-noise ratio in the detected difference frequency in

1. Optical Communication
2. Heterodyne detection
3. Lasers, Single mode

I. AFSC Project 4519 Task 451905
II. Contract AF30 (602)-2591
III. Technical Research Group Inc. Syosset, N.Y.
IV. J.Latourrette, S.Jacobs, G.Gould

Rome Air Development Center, Griffiss AF Base, N.Y.
Rpt.No. RADC-TDR-62-491. HETERODYNE DETECTION IN OPTICAL COMMUNICATION. FIRST TECHNICAL NOTE.
30 Nov. 62, 141p., incl. illus., tables.

Unclassified Report

The properties of optical heterodyne detection are analyzed and measured using a LASER and a Twyman-Green interferometer. It is shown that heterodyne amplification preserves the signal-to-noise ratio in the detected difference frequency in

1. Optical Communication
2. Heterodyne detection
3. Lasers, Single mode

I. AFSC Project 4519 Task 451905
II. Contract AF30 (602)-2591
III. Technical Research Group Inc. Syosset, N.Y.
IV. J.Latourrette, S.Jacobs, G.Gould

the presence of incoherent noise. The uses of heterodyne detection in optical communication, demultiplixing of channels, demodulation of FM and AM, Doppler and displacement measurements, and stabilization of LASERs is discussed; LASERs, Modulators transmission path, and detectors. Recommendations are made for future work.	V. Secondary Rpt. No. TRG 168-TDR-1 VI. Not available fr. OTS. VII. Available in ASTIA collection.	the presence of incoherent noise. The uses of heterodyne detection in optical communication, demultiplixing of channels, demodulation of FM and AM, Doppler and displacement measurements, and stabilization of LASERs is discussed; LASERs, Modulators transmission path, and detectors. Recommendations are made for future work.	V. Secondary Rpt. No. TRG 168-TDR-1 VI. Not available fr. OTS. VII. Available in ASTIA collection.
the presence of incoherent noise. The uses of heterodyne detection in optical communication, demultiplixing of channels, demodulation of FM and AM, Doppler and displacement measurements, and stabilization of LASERs is discussed; LASERs, Modulators transmission path, and detectors. Recommendations are made for future work.	V. Secondary Rpt. No. TRG 168-TDR-1 VI. Not available fr. OTS. VII. Available in ASTIA collection.	the presence of incoherent noise. The uses of heterodyne detection in optical communication, demultiplixing of channels, demodulation of FM and AM, Doppler and displacement measurements, and stabilization of LASERs is discussed; LASERs, Modulators transmission path, and detectors. Recommendations are made for future work.	V. Secondary Rpt. No. TRG 168-TDR-1 VI. Not available fr. OTS. VII. Available in ASTIA collection.

Rome Air Development Center, Griffiss AF Base, N.Y.
Rpt.No. RADC-TDR-62-491. HETERODYNE DETECTION IN OPTICAL COMMUNICATION. FIRST TECHNICAL NOTE.
30 Nov. 62, 141p., incl. illus., tables.

Unclassified Report

The properties of optical heterodyne detection are analyzed and measured using a LASER and a Twyman-Green interferometer. It is shown that heterodyne amplification preserves the signal-to-noise ratio in the detected difference frequency in

1. Optical Communication
2. Heterodyne detection
3. Lasers, Single mode

I. AFSC Project 4519 Task 451905
II. Contract AF30 (602)-2591
III. Technical Research Group Inc. Syosset, N.Y.
IV. J.Latourrette, S.Jacobs, G.Gould

Rome Air Development Center, Griffiss AF Base, N.Y.
Rpt.No. RADC-TDR-62-491. HETERODYNE DETECTION IN OPTICAL COMMUNICATION. FIRST TECHNICAL NOTE.
30 Nov. 62, 141p., incl. illus., tables.

Unclassified Report

The properties of optical heterodyne detection are analyzed and measured using a LASER and a Twyman-Green interferometer. It is shown that heterodyne amplification preserves the signal-to-noise ratio in the detected difference frequency in

1. Optical Communication
2. Heterodyne detection
3. Lasers, Single mode

I. AFSC Project 4519 Task 451905
II. Contract AF30 (602)-2591
III. Technical Research Group Inc. Syosset, N.Y.
IV. J.Latourrette, S.Jacobs, G.Gould

Rome Air Development Center, Griffiss AF Base, N.Y.
Rpt.No. RADC-TDR-62-491. HETERODYNE DETECTION IN OPTICAL COMMUNICATION. FIRST TECHNICAL NOTE.
30 Nov. 62, 141p., incl. illus., tables.

Unclassified Report

The properties of optical heterodyne detection are analyzed and measured using a LASER and a Twyman-Green interferometer. It is shown that heterodyne amplification preserves the signal-to-noise ratio in the detected difference frequency in

1. Optical Communication
2. Heterodyne detection
3. Lasers, Single mode

I. AFSC Project 4519 Task 451905
II. Contract AF30 (602)-2591
III. Technical Research Group Inc. Syosset, N.Y.
IV. J.Latourrette, S.Jacobs, G.Gould

Rome Air Development Center, Griffiss AF Base, N.Y.
Rpt.No. RADC-TDR-62-491. HETERODYNE DETECTION IN OPTICAL COMMUNICATION. FIRST TECHNICAL NOTE.
30 Nov. 62, 141p., incl. illus., tables.

Unclassified Report

The properties of optical heterodyne detection are analyzed and measured using a LASER and a Twyman-Green interferometer. It is shown that heterodyne amplification preserves the signal-to-noise ratio in the detected difference frequency in

1. Optical Communication
2. Heterodyne detection
3. Lasers, Single mode

I. AFSC Project 4519 Task 451905
II. Contract AF30 (602)-2591
III. Technical Research Group Inc. Syosset, N.Y.
IV. J.Latourrette, S.Jacobs, G.Gould

the presence of incoherent noise. The uses of heterodyne detection in optical communication, demultiplixing of channels, demodulation of FM and AM, Doppler and displacement measurements, and stabilization of LASERs is discussed; LASERs, Modulators transmission path, and detectors. Recommendations are made for future work.	V. Secondary Rpt. No. TRG 168-TDR-1 VI. Not available fr. OTS. VII. Available in ASTIA collection.	the presence of incoherent noise. The uses of heterodyne detection in optical communication, demultiplixing of channels, demodulation of FM and AM, Doppler and displacement measurements, and stabilization of LASERs is discussed; LASERs, Modulators transmission path, and detectors. Recommendations are made for future work.	V. Secondary Rpt. No. TRG 168-TDR-1 VI. Not available fr. OTS. VII. Available in ASTIA collection.
the presence of incoherent noise. The uses of heterodyne detection in optical communication, demultiplixing of channels, demodulation of FM and AM, Doppler and displacement measurements, and stabilization of LASERs is discussed; LASERs, Modulators transmission path, and detectors. Recommendations are made for future work.	V. Secondary Rpt. No. TRG 168-TDR-1 VI. Not available fr. OTS. VII. Available in ASTIA collection.	the presence of incoherent noise. The uses of heterodyne detection in optical communication, demultiplixing of channels, demodulation of FM and AM, Doppler and displacement measurements, and stabilization of LASERs is discussed; LASERs, Modulators transmission path, and detectors. Recommendations are made for future work.	V. Secondary Rpt. No. TRG 168-TDR-1 VI. Not available fr. OTS. VII. Available in ASTIA collection.